Politecnico
di Torino

1859

UNIVERSITAT DE
BARCELONA

IBEC
Institute for Bioengineering of Catalonia

EXCELENCIA
SEVERO
OCHOA

Master of Science in Biomedical Engineering

October 2021

Study of the feasibility of a soft gelatin methacryloyl-based template to develop cell-derived matrices for screening patients with congenital muscular dystrophies

Supervisors:

Oscar Castaño Linares

Valeria Chiono

Enrico Almici

Candidate:

Vanessa Chiappini

Index of Abbreviations

3D: Three dimensional

AlgMA: Alginate methacrylate

CDM: cell-derived matrix

COL6-RD: Collagen VI related congenital muscular dystrophies

GelMA: gelatin methacryloyl

H-NMR: proton nuclear magnetic resonance

Index

I. Abstract

Collagen VI-related muscular dystrophies (COL6-RD) are a family of rare diseases associated with collagen VI deficiency, such as the severe Ullrich Congenital Muscular Dystrophy or the intermediate forms of Bethlem Myopathy. The life quality of patients with COL6-RD is highly reduced, due to disabling symptoms, such as respiratory insufficiency, weakness, loss of independent mobility, and joint contracture. Overall, life expectancy is highly decreased, but, to date, there is no effective therapy. Dominant or recessive mutations in one of the three collagen VI genes are considered to be the onset of these diseases. The integrity of the fibrillar network of the collagen VI is lost, altering the incorporation in the extracellular matrix (ECM) and disrupting tissues homeostasis. Recent studies have revealed that patients' fibroblasts can be employed to explore the pathological characteristics of ECM related to COL6-RD, but further analyses are required to understand the mechanisms that regulate COL6-RD and ECM alterations at the molecular level. Hence, *in vitro* studies of the pathological ECM are required to investigate new screening methods and new therapeutic strategies.

In this work, three different substrates for cell-derived matrices (CDMs) production were compared. In particular, a gelatin coating, previously employed in studying ECM fibrillar properties of healthy donors and patients, was juxtaposed to a novel gelatin methacryloyl (GelMA) and alginate methacrylate (AlgMA) interpenetrating polymer network (IPN) in form of a hydrogel. Indeed, the flat 2D microenvironment sensed by cells in the gelatin coating may limit the study of cells' morphology, migration, and interaction with the produced ECM. Therefore, two configurations were investigated: a hydrogel with a monolayer of mouse fibroblasts seeded on the top and a three-dimensional cell-laden hydrogel with a specific thickness. Indeed, developing a 3D CDM construct using patients' fibroblasts should further replicate the complex structure of tissues, allowing a more accurate analysis in a biomimetic environment. However, when cells were surrounded by the gel, viability was high, but fibronectin and collagen production diminished, suggesting cell suffering. In conclusion, in this previous study of CDMs, the 2D configuration resulted in being the better option for screening patients. Still, more investigations have to be carried out to obtain a 3D construct to help understand the mechanism of these rare diseases and develop new treatments.

1. Introduction

1.1 Collagen VI related congenital muscular dystrophies (COL6-RD)

COL6-RDs are the second most common form of congenital muscular dystrophies with a prevalence between 0,1 and 0,5 per 100,000, and consists of a heterogeneous family of rare neuromuscular disorders associated with mutations in collagen VI genes [1], [2]. Collagen VI is a non-fibrillar component of the extracellular matrix (ECM), mostly secreted by fibroblasts, which is implicated in tissue organization. Indeed, collagen VI is closely related to numerous ECM components, such as fibronectin, fibrillar collagens I and II, proteoglycans, and glycosaminoglycans [3]. Therefore, clinical hallmarks of COL6-RD are associated with alterations in patients' connective tissue. COL6-RDs enclose various clinical conditions, from the severe Ullrich Congenital Muscular Dystrophy (UCMD, OMIM 254090) to the intermediate forms of Bethlem Myopathy (BM, OMIM 158810). UCMD patients are affected by proximal muscle weakness, proximal joint contractures, delayed motor milestones, hypotonia and distal joint hyperlaxity [4]. At the severe stage of the UCMD spectrum, most patients never walk independently: only a few children acquire this ability, but with the progression of the disease, ambulation is early loss. Common features are also feeding difficulties in childhood and nocturnal respiratory insufficiency requiring nocturnal non-invasive ventilation. Overall, life expectancy is highly decreased. Instead, due to the milder entity of BM, patients present a slower progression of the symptoms, even showing independent ambulation in adulthood [5], [4].

Collagen VI is composed of three α chains, α1, α2 and α3 forming a heterotrimeric monomer, further associated into antiparallel dimers by disulfide bonds between cysteine residues and aligned laterally into tetramers. These tetramers are assembled in an end-to-end fashion: the final microfilament network (Figure 1).
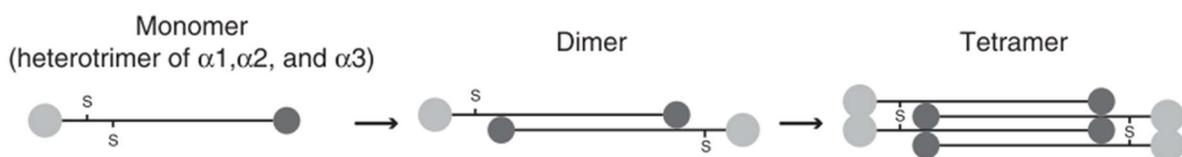
Figure 1. Collagen VI structure. It is highlighted the assembly of the three alpha chains in a monomer, the antiparallel association of monomer in a dimer stabilized by disulfide bonds and the final parallel association in the tetramer. Reprinted from [6].

Dominant or recessive mutations in one of the three genes, COL6A1, COL6A2, and COL6A3, alter the structure (observable with the electron microscope [6]) or functionality of collagen VI tetramers, which leads to a partial deficiency or a total absence of collagen VI in the connective tissue [5]. Nonetheless, it is still unclear the link between the mode of inheritance, the extent of collagen VI reductions, and patients' phenotype. Consequently, it is necessary to continue investigating the mechanisms underlying this disease to better understand the effects of collagen VI deficiency and altered ECM structure on patients' progression.

1.2 Extracellular matrix

Tissues are composed of many different types of cells and the extracellular matrix (ECM). The ECM sustains suitable conditions for cells homeostasis and tissue structural integrity [7]. It is composed of a heterogeneous network of polysaccharides, proteins, and glycosaminoglycans, which drive cell adhesion, differentiation, migration, proliferation, homeostasis, and apoptosis [8]. Thanks to receptors and growth factors, cells activate signalling cascades and gene transcription, allowing the dynamic remodelling of the ECM [8]. Therefore, the relationship between cells and ECM is dynamic, and they can remodel and influence each other.

The main components of the ECM are fibrous proteins, like collagen, elastin, and fibrillin, adhesive glycoproteins, such as laminin, integrin, fibronectin, and glycosaminoglycans. Moreover, it is composed of a high amount of water. It has a crucial role in the diffusion of oxygen and nutrient and the removal of waste products. Every cell and tissue type produces its own ECM, which is probably unique in terms of composition. Biophysical properties, such as stiffness, porosity, and topography, are tissue-specific and influence the surrounding cells in homeostasis and morphogenesis [9].

1.3 Cell-derived matrix

Historically, cell biology studies have been performed in rigid 2D cell culture conditions that lack many features of the *in vivo* cellular environment. Nowadays, it is clear that cell behaviour and homeostasis are influenced by environmental cues, which include the extracellular compartment and its biochemical and biophysical properties. Increasing studies focus on mimicking *in vitro* the 3D nature of *in vivo* microenvironments. Natural and

synthetic materials, along with several processing techniques, have been proposed to mimic the properties of native tissues. Nonetheless, they systematically fail in reproducing the complex architecture and composition of the ECM [10].

The main sources of structured ECM *in vitro* are derived from the decellularization of tissue and organs [11]. Decellularized ECM from native tissue has the main advantages to keep the vascular network and the 3D native complex architecture. Nonetheless, maintaining the properties of the tissue is difficult, due to the harsh conditions necessary to ensure complete decellularization. Moreover, after decellularization, the homogeneous repopulation of the entire structure is often critical. Furthermore, lack of tissues and donors, critical immunogenicity, batch-to-batch variability are considerable limitations. In this scenario, decellularized cell-derived matrices (CDM) have been proposed to recapitulate the complexity of the ECM *in vitro* [8]. CDM consists of a structured scaffold of ECM proteins that elicit in vivo-like response in cultured cells and it can be employed as an ECM model of patients' tissues. CDMs are produced by culturing *in vitro* immortalized or primary cells in controlled conditions for a specific period of time before decellularization [12].

This method provides several advantages: first, it is a personalized strategy that has unlimited availability. Second, cells can be screened, avoiding contamination, and they are maintained in a pathogen-free condition [8]. Third, it is possible to use a wide range of cell types or genetically modify them to tailor the fabricated structure's properties. Fourth, CDM can be prepared with the desired geometry, simplifying the decellularization process compared to the whole tissues and avoiding problems during the repopulation of the environment. Furthermore, CDMs allow mixing different cell lines, including autologous cells, creating a coculture and producing a broad range of microenvironments. Nonetheless, CDMs still present limitations such as low 3-dimensionality, low scalability, and difficult handling. By exploiting scaffolding materials it is possible to control and tailor the properties of the resulting CDM [8], [13].

Several biomaterials have been proposed to support cells during the secretion of matrices: from synthetic templates to natural polymers. Indeed, to reconstruct three-dimensionality, cells can be seeded in a scaffold of various compositions and geometries — for instance, electrospun polycaprolactone (PCL) microfibers, titanium fibrous mesh, or microencapsulated collagen fibers. Recently, CDM research has highly increased, involving

4

different types of study and analysis, such as fabrication processes, best cell type for production, and characterization. Indeed, numerous factors can be tailored to mimic the natural target tissues properly.

CDMs have a comprehensive range of applications. A precise analysis of cell processes, such as adhesion, migration, viability, proliferation, and differentiation, can be carried out. The broad set of different culture conditions and approaches make this technique extremely powerful.

CDMs are promising methods for studying tissue morphology and pathological alteration [14]. They can be employed as disease models for testing personalized treatments and reproduce *in vitro* patients' heterogeneity [8].

1.3.1 CDMs fabrication methods

Continuous development of new techniques has increased the possibility of bottom-up fabrication methods for CDMs. Choose the fabrication methods is a critical step of the process because it highly influences ECM properties. Moreover, several parameters require control in order to fabricate CDMs with specific characteristics: (i) cell source, (ii) culture substrate, (iii) medium composition, (iv) decellularization process, and (v) physical and chemical modifications [15].

The cell source impacts on the architecture and composition of CDMs, because different proteins can be secreted by different cells [15]. Regarding the supporting substrate, gelatin and fibronectin coatings are usually employed because they ensure CDM stability [15]. Often, in more complex system, a combination with hydrogel or polymeric materials may be required, especially when long-term mechanical support or a specific stiffness is needed [8].

The medium composition can highly influence CDMs production. For instance, it has been demonstrated that NIH-3T3 fibroblasts produce thicker matrices in the presence of calf serum [16].

Several ways of decellularization have been investigated: chemical agents, physical or enzymatic treatment. Indeed, it is fundamental to optimize the protocol to achieve CDMs with low DNA contamination.

1.3.2 CDMs characterization

A thorough characterization of CDMs produced is necessary to understand cells behaviour or disease progression. Indeed, engineering CDMs advantage is to provide a system that can be analysed with deep spatio-temporal resolution. A broad range of assays can be implemented to investigate CDMs composition and architecture.

First of all, DNA is normally detected through cell nuclei staining (e.g. Hoechst 33258/33343 staining). Then, intracellular components can be monitored with fluorescent-labelled phalloidin to detect fibrous actin and immunocytochemistry can be employed for cytosolic proteins. Histological techniques are used for monitoring non-nucleic components or glycosaminoglycans, and immunohistochemistry is employed for specific ECM components. Moreover, cells that secrete fluorescent proteins can be used to produce fluorescent CDMs [15]. Additionally, quantification can be carried out using multiple methods, such as in situ enzyme-linked immunosorbent assays (ELISA), sodium dodecyl sulfate-polyacrylamide gel electrophoresis (SDS-PAGE) or Western blots [8].

It is well-known that mechanical properties are critical in influencing cell signalling and ECM production. In particular, stiffness and viscoelasticity are the main properties to evaluate since they affect cell differentiation and growth. The first one can alter mechanotransduction, while the second one can modify the ability of cells to remodel CDM. They can be assessed with compression and rheometer machines, while atomic force microscopy (AFM) is employed to locally measure the spatial heterogeneities of CDMs [15].

Alongside these characterizations, morphological properties of the CDMs produced have to be accurately investigated through scanning electron microscopy (SEM) and software such as ImageJ, MATLAB, and CT-FIRE [8].

1.4 Improving CDMs three-dimensionality

Previous works have thoroughly investigated collagen VI deficiency production in patients' fibroblasts, providing valuables information, but failing to reproduce the complex three-dimensional structures that characterize *in vivo* environment. In the last years, several techniques have been investigated for 3D CDM production. For instance, production of cell sheets was one of the first methods implemented (figure 2-A). Okano and colleagues developed a poly(N-isopropylacrylamide) (PIPAAm)-coated surface where cells were cultured. When cells had secreted enough ECM, samples were cooled below 32 °C, and

PIPAAm became hydrophilic. Therefore, rapid hydration induced the release of cells and ECM. Lastly, the amphiphilic PIPAAm did not damage the fabricated ECM during the decellularization process. Next, this strategy can be implemented to stacks many CDMs, achieving a thick 3D CDM [17].

The use of microparticles (MP) is an interesting way to introduce three-dimensionality into CDMs (figure 2-B). For instance, Tour *et al.* evaluated the properties of hydroxyapatite microparticles as a scaffold. Primary rat calvaria osteoblasts and dermal fibroblasts were seeded into microparticles and cultured for CDM production. After decellularization, the construct was implanted in a rat defect, and enhanced bone repair compared to the bare hydroxyapatite scaffold was shown [18].

Another widely used processing method is electrospinning (figure 2-C). Electrospinning is an advantageous and low-cost technique to produce engineering and biomimetic nanofibrous scaffolds that reproduce ECM properties. Remarkable work from Zhou *et al.* demonstrated that CDMs encourage peripheral nerve repair. Mouse fibroblasts were seeded onto electrospun poly(L-lactic acid) (PLLA) fibers and electrochemically deposited polypyrrole (PPy) nanoparticles and, after ECM production, decellularized. Afterwards, PC12 cells were seeded onto the construct. Then, differentiation, protrusion, and alignment were evaluated. A considerable improvement of properties that promote nerve regeneration was achieved [19]. Other feasible techniques for fabricating CDMs include 3D printing, culturing cells on the printed polymer surface, or mixing cells with the ink to be printed.

Overall, developing a 3D CDM construct using patients' fibroblasts should replicate closer the complex structure of tissues, allowing a more accurate analysis in a biomimetic environment. Indeed, it has been evidenced that 2D substrates do not mimic properly in vivo environments, consequently failing to express tissue-specific genes and proteins. Therefore, introduce three-dimensionality to CDM is essential. As support for CDMs production, hydrogels are a great option from the wide range of available materials, thanks to a network that partially resembles characteristics of native ECM [20].
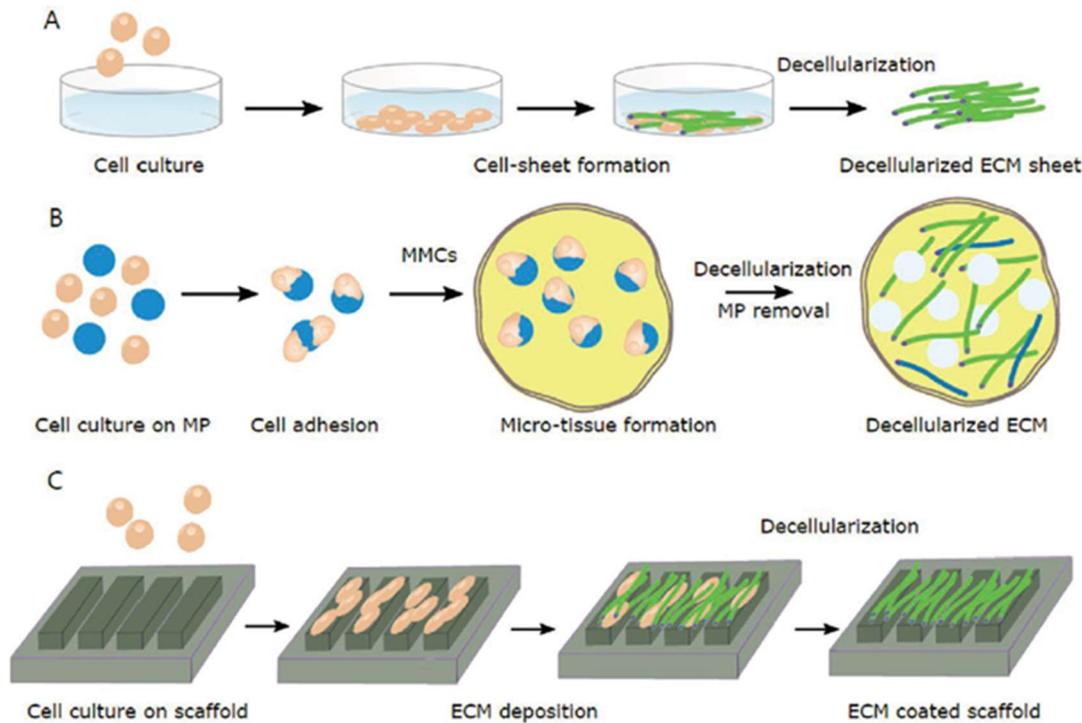
Figure 2. Fabrication strategies for CDMs production. Cells are cultured to produce A) ECM sheets, B) microtissues by microparticles, and C) tissues on a 3D scaffold. Reprinted from [8].

1.5 Hydrogels

In the last decades, hydrogels have gained increased interest in various applications, including the biomedical field. According to the definition given by Peppas, hydrogels are cross-linked polymeric three-dimensional networks, able to hold a significant amount of water and with covalent bonds between co-monomers, cross-links of chain entanglements and strong Van der Waals interaction or hydrogen bonds between chains [21]. Hence, hydrogels as 3D systems and water-solvated can swoll and their mechanical properties are modulated, being suitable for the fabrication of biomimetic structures. Indeed, high water content and an exceptionally soft and rubbery consistency allow hydrogels to mimic native ECM of tissues closely [17].

The first application of hydrogels in the biomedical field dates back to 1960 when Wichterle and Lim produced a soft contact lens material of cross-linked poly(2-hydroxyethyl methacrylate) (pHEMA). From this moment, hydrogels have attracted more and more interest, and the number of publications in this field has increased exponentially (Figure 3) [22]. Nowadays, hydrogels are the biomaterials most widely used in tissue bioengineering as 3D support for *in vitro* cell culture [23].
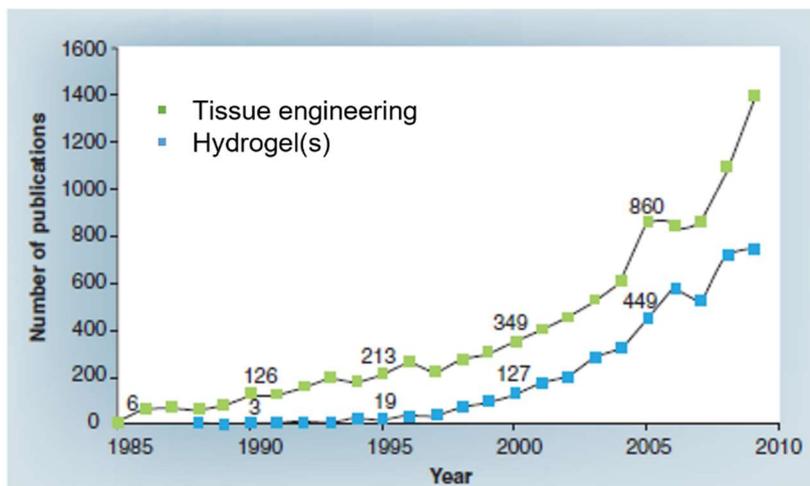
Figure 3. Number of publications from 1985 until 2010 with the words 'tissue engineering' and 'hydrogel'. Reprinted from [20].

1.5.1 Properties

Hydrogels have found widespread biomedical application mainly due to their tunable properties. The most attractive features of hydrogels are the large amount of water they can hold and their hydrophilic behaviour: these facilitate nutrient and waste diffusion transport. Polymers used to create hydrogels can be from natural or synthetic precursors. Natural polymers, such as collagen or gelatin, have in their chains biochemical cues that influence and improve cell attachment, growth, and migration. Nonetheless, they are highly biocompatible and biodegradable. Depending on the type of hydrogel, degradation can be governed by different mechanisms (hydrolysis, enzymatic degradation or oxidation, basically). The degradation process in protein-based hydrogels such as collagen or gelatine is performed by the enzymatic action from metalloproteinases secreted by cells. This process allows matrix remodelling, leading to proliferation and migration. On the contrary, synthetic precursors lack bioactive molecules and are biologically inert but show broad physical properties that can achieve almost every specific tissue characteristic. Modifying synthetic hydrogels with peptides is often required to overcome the absence of biological cues [23]. Regarding mechanical properties, hydrogels have a midway behaviour between viscous liquids and solids. Before cross-linking, the pre-polymer solution is a Newtonian fluid. Then, hydrogels show viscoelastic behaviour. Only particular materials can reach purely elastic properties. Different factors influence mechanical properties: the polymerization degree, the origin and the type of monomer, the gelation mechanism. Therefore, physio-chemical and mechanical properties can be finely adjusted, changing these characteristics or even mixing one or more polymers.

Hydrogels are biodegradable, thanks to labile bonds present in the backbone or the polymer cross-links. Tune the composition of hydrogel in order to achieve the desired degradation time is significantly important because hydrogel degradation must be replaced by ECM production gradually while it acts as a template.

Another remarkable characteristic is biocompatibility. Material biocompatibility is the property to act as a substrate able to support cellular growth without systemic or local effects in the host. Good biocompatibility is mainly due to the polymer origin (natural or synthetic) or the addition of cytotoxic agents, such as photoinitiators, during the gelation mechanism. Nevertheless, thanks to a significant amount of water content, biocompatibility is easily achievable [24].

1.5.2 Classification

Various parameters should be taken into account for hydrogel classification: origin, method of preparation, physical properties, rate of biodegradation, ionic charge, or nature of cross-linking (figure 4). Nonetheless, three subclasses are typically used to categorized and distinguish hydrogels: material of origin, cross-linking method, and responsiveness to external stimuli [25].

Origin material is the first hydrogels classification. They are divided into natural, synthetic or hybrid polymers.
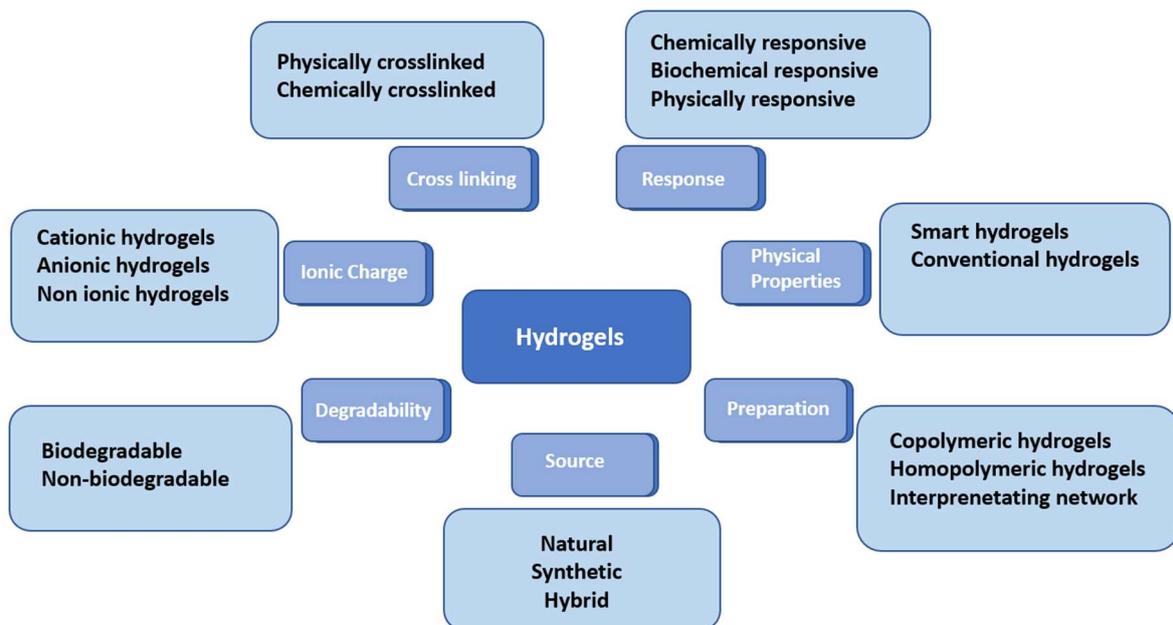
Figure 4. Several ways to classify hydrogels. Adapted from [25].

Natural polymers are acquired from natural sources. Derived from polysaccharide polymers or proteins, they are biocompatible and bioactive. Indeed, natural gels are mainly formed by ECM components, such as collagen, hyaluronic acid, fibrin, or are a mixture of ECM proteins, like Matrigel. Moreover, materials derived from other biological sources are employed: chitosan, silk fibril, or alginate, among others. On the one hand, natural gels promote cell viability and proliferation thanks to a high affinity for protein, particularly integrins and fibronectin. On the other hand, good mechanical properties and high stiffness are often challenging to achieve. Moreover, they have batch-to-batch variability because they are extracted from natural tissues, but this is not a limiting factor thanks to high-quality control of the extracted polymer available nowadays [23], [26].

A wide range of synthetic materials is currently employed to create scaffolds for tissue engineering. Poly(ethylene glycol) (PEG), poly-α- hydroxy acids (polylactic acid, PLA and polyglycolic acid, PGA), and poly(ε-caprolactone) (PCL) have demonstrated to be successful as biocompatible and biodegradable templates with high viability also in 3D cell culture. These biodegradable polymers are simply processed and highly reproducible, allowing stiffness and mechanical properties tuning. However, they lack bioactivity to promote cell adhesion and proliferation and their stiffness is still too high, especially for soft tissue applications. Several strategies of functionalization to reach a bioactive structure have been investigated to overcome the lack of bioactivity. Functionalization introduces various peptides in the material backbone that promotes the desired features (adhesion, specific differentiation) [26].

Cross-linking classification divides hydrogels into two groups: chemical or physical cross-linking. Physically cross-linked hydrogels usually are composed of graft copolymers and multiblock copolymers. Physical interactions include the formation of hydrogen, electrostatic, hydrophobic, or ionic bonds between the polymer chains. All these interactions are weak and non-stable. Although synthetic and natural polymers can be used to create physically cross-linked hydrogels, the most employed source is the second one. A way to reach a physical cross-link is a sol-to-gel transition that occurs varying the temperature. The sol-to-gel transition is due to the presence of hydrophobic and hydrophilic blocks in the polymeric chains that form micelle and pack into a network. The polymer's hydrophilic/hydrophobic content rate and the length of chains modulate the temperature

phase transition. For instance, Matrigel jellifies when the temperature is increased. Another way to obtain physically cross-linked hydrogels is thanks to ionic interactions. Ionic interactions occur between a charged polymer and a charged molecule. This process can be carried out at physiological pH and room temperature, avoiding cell viability problems due to high or low temperatures. The most well-known material with physical cross-linking is alginate, which can cross-link in the presence of Ca^{2+}. Moreover, it is possible to fabricate physical hydrogels due to hydrogen bonds between two polymeric chains. Overall, interest in physically cross-linking agents is in expansion, mainly because toxic agents are avoided. Chemical cross-linked hydrogels form covalent bonds between chains, resulting in a stable network permanently cross-linked. Chemical cross-linking is reached in several ways: by radical polymerization, enzymatic polymerization, condensation reactions, high-energy irradiation, or chemical reactions between complementary groups. The first mechanism is the most widely employed, and it requires the addition of a crosslinker with specific properties. Photo-initiator and low molecular weight side groups or monomers activated in free radicals upon UV form several covalent solid bonds that macroscopically result in a hydrogel. Electron and gamma beams are employed for cross-linking involving high-energy irradiation, but the toxicity of the process has to be controlled before encapsulating cells. Overall, covalent bonds typic of chemical cross-linking provide greater mechanical stability than physically cross-linked hydrogel [25].

Stimuli-responsive gels can respond to environmental stimuli of different nature, changing their structure, permeability, or mechanical properties. pH, chemical agents, or ionic factors are chemical stimuli able to change the interactions in the hydrogels at the molecular level. Light, electric or magnetic fields, temperature, or pressure at precise settings can change molecular interactions, giving a physical stimulus. Biochemical agents, enzymes, or antigens can also produce a biochemical stimulation. A combination of two stimuli is also achievable, and in this case, the polymer is called 'dual responsive'. In conclusion, if the properties are fine-tuning, a wide range of applications is feasible for the stimuli-responsive hydrogel, particularly in the pharmaceutical field [25].

1.5.3 Polymerization mechanisms

Polymerization is the reaction between monomer chains in a solution to form a three-dimensional network. Two types of polymerization mechanics exist step-growth and chain

growth. The first mechanism is like a click reaction, and any monomer or oligomer with a functional group reacts independently with other active groups. Polymerization starts with the development of dimers from monomers. Then, chains increase in length until a high molecular weight is reached (figure 5-a). High molecular weight in this mechanism is achieved in the reaction's final times when polymers and oligomers react with each other's. In fact, there is a slow increase of molecular weight at the beginning of the process when monomers are consumed.
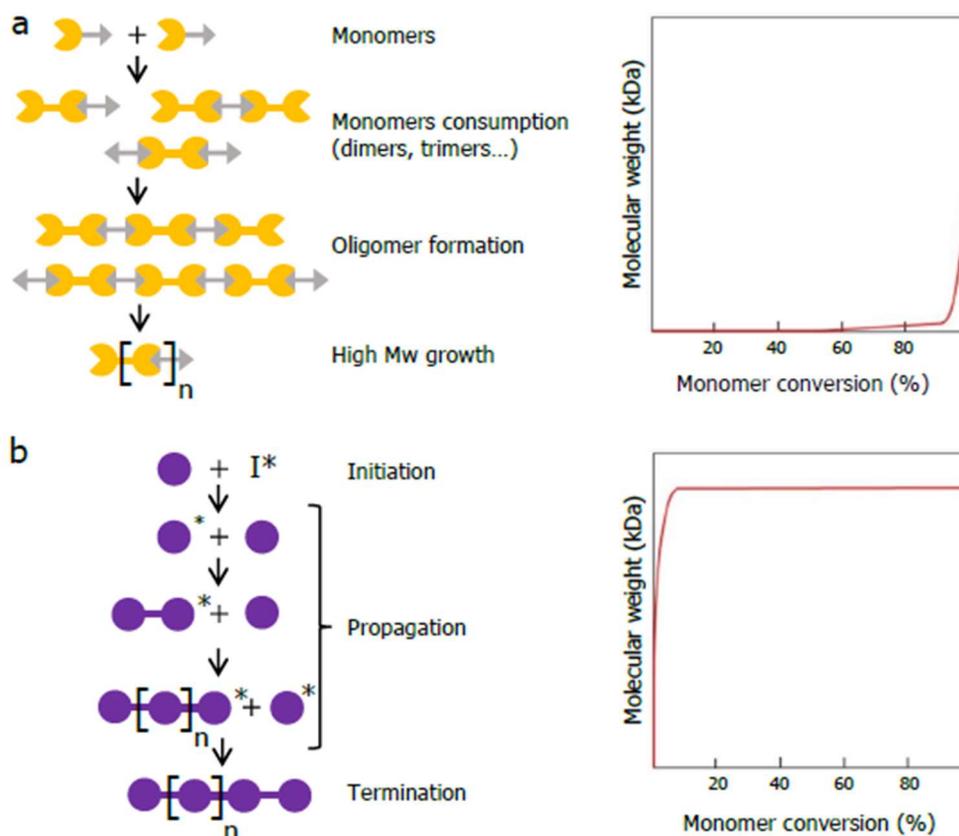
Figure 5. It is shown a schematic illustration of polymerization mechanism (left panel) and polymerization conversion percentage versus molecular weight of the A) step-growth polymerization and B) chain growth polymerization. I* represent a radical of the photoinitiator. Reprinted from [9].

In this mechanism, add an external molecule to commence the reaction is not necessary [27]. Instead, in chain-growth polymerization, just previously activated functional groups can react with monomers. The functional activation of chemical groups is called the initiation step. Next, during the propagation step, the center of reaction is the end of the chain that continues to react until reactive centers are consumed. This time is known as the termination step (figure 5-b). Contrary to step-growth, this process led rapidly to high

molecular weight. Predominantly, the reaction rate is influenced by initiator concentration and its efficiency.

1.5.4 Photo-curable hydrogels

A process known as photopolymerization is a process where a polymer solution is mixed with a photosensitive molecule (i.e. photoinitiator) and converted to a 3D hydrogel by the chain-growth reaction. Like chain-growth polymerization, this process is divided into three steps: initiation, propagation and termination. Compared to the other mechanisms to form hydrogels, free radical polymerization has many advantages, including mild conditions during all the protocols (room temperature, neutral pH, aqueous solution), proper Spatio-temporal control and high speed of reaction, decreasing cell suffering. For these reasons, it is often preferred in the biomedical field. In free-radical photopolymerization, photoinitiator and polymer solution react under visible or UV light. UV-irradiated hydrogels have been more investigated mainly because they can introduce a high number of covalent bonds in a shorter time due to the high energy of irradiation. However, precisely the high energy can damage cells and may not be ideal for tissue applications. On the contrary, visible light (wavelengths between 400 and 700 nm) is less toxic [28], [29].

Photoinitiator absorbs the light, generating free radicals to start the process. Radical photoinitiators are divided into two classes, type I and type II. Type I or cleavage-type photoinitiators, such as Lithium Phenyl(2,4,6-trimethylbenzoyl)phosphinate (LAP) and 1-[4-(2-hydroxyethoxy)-phenyl]-2-hydroxy-2-methyl-1-propanone (Irgacure D-2959), acquire photons and, starting the reaction, decay into two free radicals. In contrast, type II photoinitiators, such as Riboflavin, eosin-Y, Rose Bengal, require a co-initiator from which they subtract one hydrogen to form secondary radicals and commence the reaction.

Regarding the suitability of a photoinitiator, the main parameters to consider are the solubility in an aqueous solution and an adequately molar absorptivity at cytocompatible wavelengths. Irgarcure-2959 has a water solubility lower than 0.5 wt% and a molar absorptivity at 365 nm lower than 10 $M^{-1} \cdot cm^{-1}$. Moreover, its molar absorptivity at visible light is near zero. On the contrary, LAP has higher water solubility (> 5 wt%) and absorbance at 365 nm ($\varepsilon \approx 200$ $M^{-1} \cdot cm^{-1}$) but still does not reach a good absorptivity at visible light ($\varepsilon \approx 30$ $M^{-1} \cdot cm^{-1}$). Conversely, type II photoinitiators have a high absorptivity at visible light and exceptional water solubility [30].

In general, as the photopolymerization conditions are often cytotoxic and harmful, it is necessary to evaluate the viability of cells after the process [24].

1.6 Gelatin methacryloyl

Gelatin methacryloyl (GelMA) derives from gelatin, and it was first synthesized by Van Den Bulcke *et al*. in 2000 [31]. Gelatin is a natural hydrophilic polymer, hydrolytically degraded from collagen but with lower aromatic groups and, therefore, lower immunogenicity (figure 6-a). Gelatin normally jellifies in an aqueous solution below about 37 °C, partially regaining the triple-helix structure typical of collagen. On the contrary, above this temperature, it is soluble in water. Moreover, gelatin maintains from collagen several bioactive sequences, such as arginine-glycine-aspartic acid (RGD motif), which foster growth and adhesion of several types of cells, and enzymes for extracellular remodelling and cell degradation, such as matrix metalloproteinase (MMP) [32]. Unfortunately, gelatin is not perfectly stable at body temperature, becoming unsuitable for many applications. Still, thanks to numerous active groups on the side chains, including -COOH, -OH, -SH and -NH$_2$, it is easy to modify to overcome its limitation [33].

GelMA hydrogels are fabricated by reacting gelatin and methacrylic anhydride (MA) (figure 6-b) in the presence of a photoinitiator. The percentage of MA employed is commonly less than 5 %; therefore, most of the bioactive motifs from gelatin are preserved [32].
GelMA concentration, percentage of MA, photo-curing times, initiator concentrations, ultraviolet (UV) dose and temperature during cross-linking are the parameters to evaluate to tailor the properties of the hydrogel, especially compressive modulus, pore size, degradation time and swelling rate [34], [35], [36], [37]. In particular, a decrease of polymer concentration, degree of functionalization and UV intensity diminish hydrogel stiffness but increase pore size and cell spreading [38], [39], [40]. Tailoring these characteristics, stiffnesses from around 1 kPa [41] to above 100 kPa [42] are achievable. Nonetheless, it is crucial to evaluate cytotoxicity depending on methacrylation degree, photoinitiator concentrations and % w/v of GelMA, parameters that may strongly affect cells viability [9], [39].

GelMA has excellent characteristics but frequently lacks a durable structure and is rapidly degraded by mammalian cells [38]. Therefore, it is often used in combination with other non-biodegradable biomaterials. In this work, to achieve a long-lasting architecture, alginate methacrylate was added.
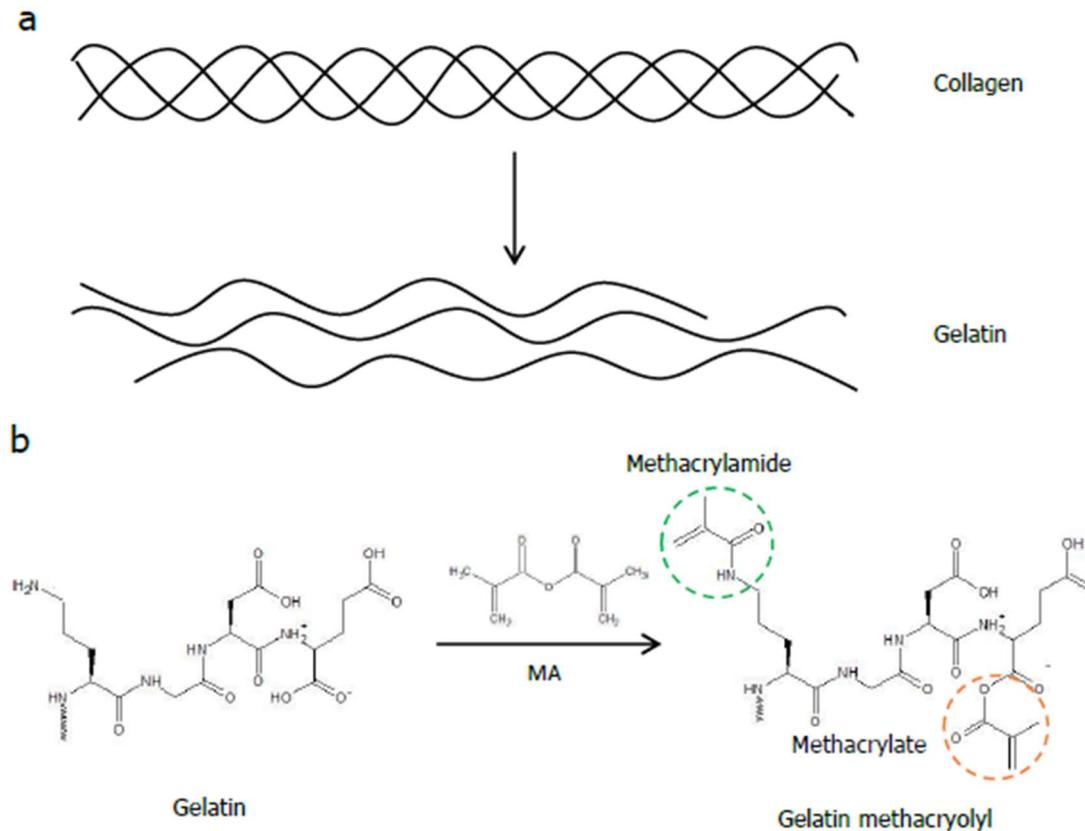
Figure 6. Synthesis of gelatin methacryloyl. A) triple helix of collagen is denaturalized into single molecules, the gelatin. B) Funcionalization of the gelatin with unsaturated methacyloyl groups by reaction with methacrylic anhydride (MA). These groups are a mixture of a majority of methacrylamide groups and a minority of methacrylate groups. Reprinted from [9].

1.7 Gelatin methacryloyl - Alginate methacrylate copolymer

Sodium alginate is a polymer extracted from brown algae (Phaeophyceae), processed with aqueous alkali solution, often NaOH and filtered with sodium or calcium chloride. Alginate is biocompatible, with low toxicity and a low cost, so widely employed in the biomedical field. In tissue engineering, alginate is usually employed in the form of hydrogel. Indeed, an aqueous alginate solution combined with ionic cross-linking agents, such as Ca^{2+}, forms an ionically cross-linked network with poor long-term stability in physiological conditions due to release in the media of divalent ions. Hence, covalent cross-linking was extensively investigated. Among others, photo cross-linking of alginate modified with methacrylate has

shown adequate properties. Alginate methacrylate (AlgMA) is non-degradable by mammalian cells, lacking the specific enzyme for breaking up the bonds [43].

Gelatin and alginate are two of the most clinically employed biomaterials. GelMA and AlgMA can covalently attach to each other through the photoactivated reaction or be self-crosslinked (figure 7). They create a hydrophilic and biocompatible microenvironment with better mechanical properties than pure GelMA hydrogel [37]. Indeed, it was shown by Tavafoghi and colleagues that Young's modulus continually grows by increasing AlgMA concentration due to a higher cross-linking density. Moreover, AlgMA presence limits the degradation rate, obtaining a more stable biomaterial and increases the swelling ratio, facilitating water entry [44], [45].
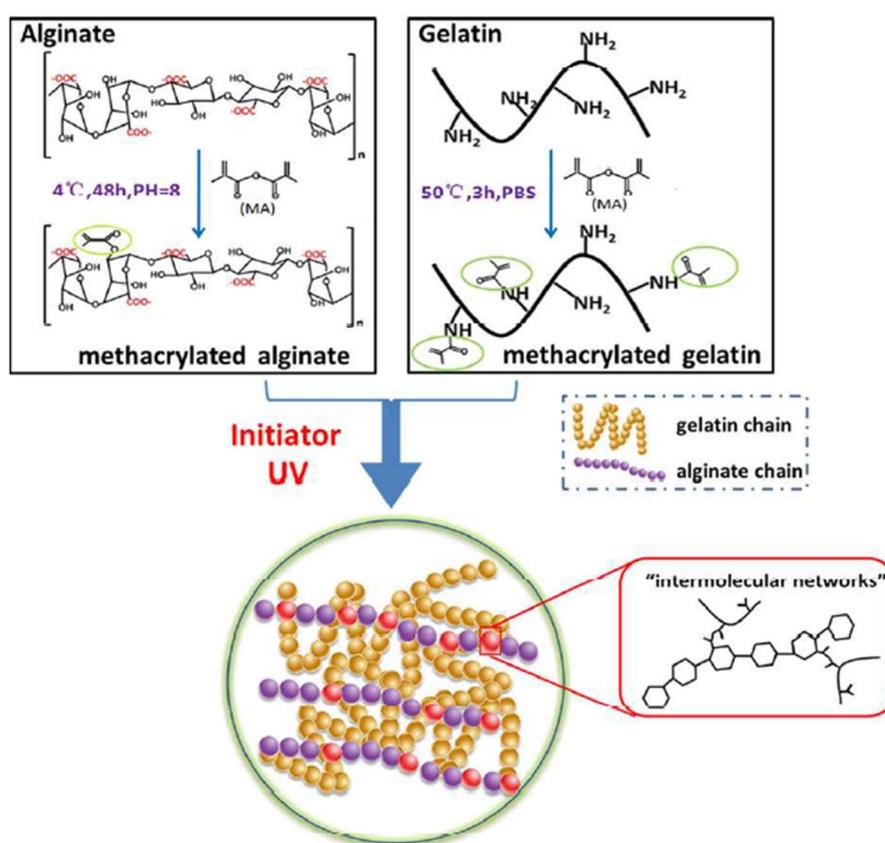
Figure 7. Schematic illustration of the gelatin methacryloyl – alginate methacrylate hydrogel synthesis. Reprinted from [45].

1.8 3D Bioprinting

3D bioprinting is a versatile and pioneering technique that allows obtaining biomimetic, functional, multi-cellular tissues and organ models from 3D digital templates [46]. The

polymer solution is mixed with the cells to fabricate the scaffold. In some cases, the prepared solution can be supplemented with other biomolecules, such as growth factors or proteins. The final solution is known as bioink. After the bioink preparation, it is dispensed in a controlled manner following a precise geometry and path and then the material employed is polymerized [46], [47].

The process is mainly composed of three steps. The pre-processing consists of the visualization by imaging of the real structure to be model through MRI, X-ray, ultrasound or CT and the template's design using specific software, for instance, SolidWorks or AutoCAD. After that, the bioprinting step is carried out. The cell-laden bioink is prepared, accurately choosing the cell type and density, and the printing parameter are selected, such as print speed, temperature, pressure. Afterwards, the bioink is printed and the biomaterial polymerized. Finally, the post-processing step provides to the structure the conditions for cells culture and growth, from the environmental conditions, such as CO_2 and temperature, to the supply of nutrients (figure 8) [46].
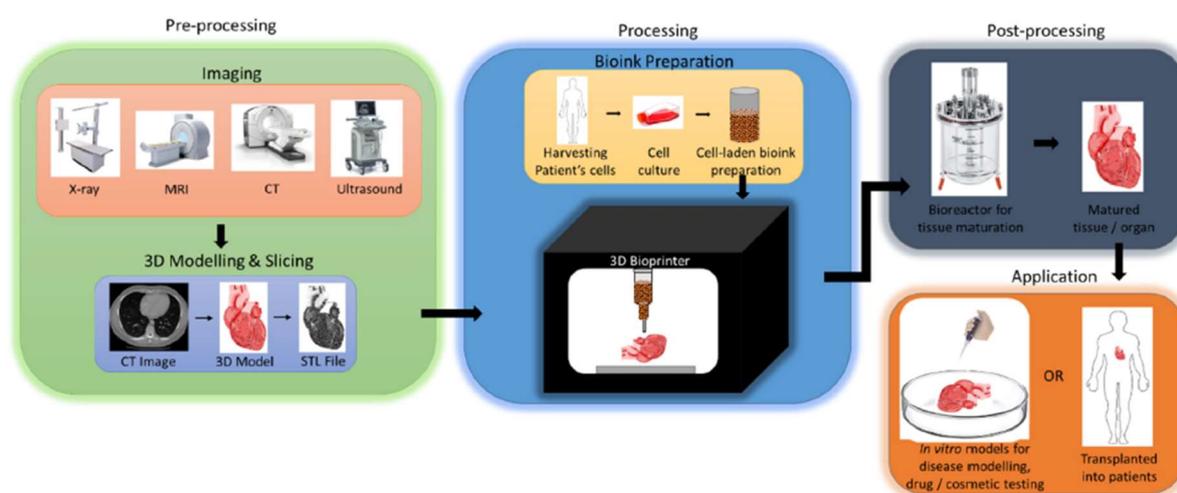
Figure 8. The bioprinting process flow. The pre-processing consists of modelling the construct. The processing consists of effective bioprinting, and post-processing provides the conditions for cell growth. Reprinted from [45].

Different 3D bioprinting technologies have been developed: (I) microextrusion, (II) inkjet and (III) laser-assisted bioprinting [48].

The most broadly employed method is microextrusion bioprinting (figure 9-b). The bioink is continuously dispensed through the nozzle, applying pneumatic or mechanical forces. Microextrusion is usually employed with a high number of cells and high viscosity bioinks. The viability after the process has to be evaluated, and generally, results compromise due to

the pressure used, resulting in elevated cellular stress. Moreover, the nozzle can be clogged. The resolution of a layer is limited to 100 µm [47].

Inkjet bioprinting is a fast, low cost and non-contact technique that employs thermal, electromagnetic or piezoelectric forces to dispense drops of bioink through the syringe (figure 9-a). This technique has high cell viability, but the droplets produced are not uniform due to the low bioink viscosity, and therefore the structure lacks homogeneity. The resolution is related to the minimum drop size, and it can be around 50 µm, but it strongly depends on how the drops spread on the surface [49].

Finally, laser-assisted bioprinting is a non-contact technique (figure 9-c). In this bioprinting technique, an absorbing layer of a ribbon is pre-coated with the bioink. The laser beam pulses on the layer generate bubbles that propel the bioink towards the substrate [47], [48]. It is a time-consuming and costly technology, but clogging is avoided because there is not a nozzle, and thus, cell viability is enhanced. Moreover, a high resolution of up to 10 µm is achieved [50].
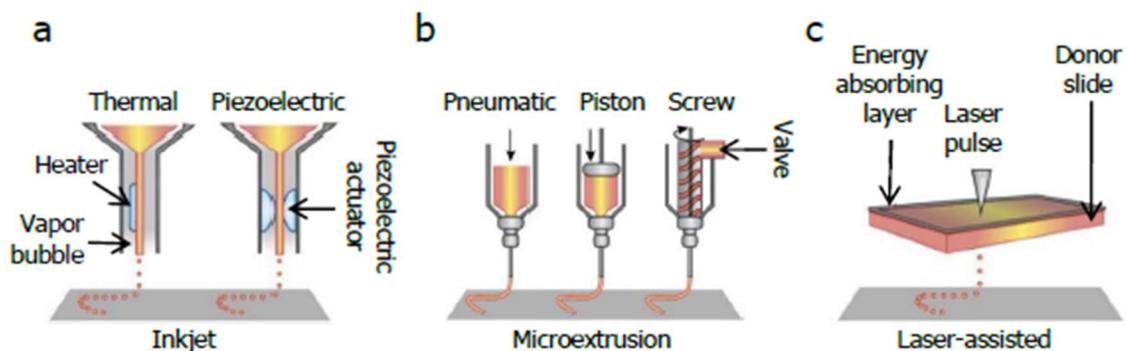
Figure 9. Mainly components of the three 3D bioprinter technologies: inkjet, microextrusion and laser-assisted bioprinter. Reprinted from [47].

2 Methods

2.1 Synthesis of gelatin methacryloyl and alginate methacrylate polymers

2.1.1 GelMA synthesis

Gelatin methacryloyl (GelMA) derives from gelatin and contains a majority of methacrylamide groups and a minority of methacrylate groups [51]. Gelatin is a denatured and, in part, hydrolyzed heterogeneous mix of collagen from animal sources [52]. It forms thermo-reversible physical interactions, but above 37 °C, gelatin hydrogels liquefy. Therefore, to obtain a stable 3D structure is commonly used GelMA, gelatin chemically modified with methacryloyl groups added to primary amine and hydroxyl groups and that, thanks to UV light, form stable covalently cross-linked hydrogels (figure 10-a) [53].

GelMA was fabricated following a method previously described [38], [9]. Briefly, gelatin of porcine skin (G1890, Sigma Aldrich, USA) was dissolved at a concentration of 10 % w/v in phosphate-buffer saline (PBS) (Sigma Aldrich) at 50°C and under stirring conditions. Then methacrylic anhydride (MA) (276685, Sigma Aldrich, USA) was thoroughly added under constant stirring. The volume of MA added determines the degree of functionalization (DoF). The methacrylation was performed in order to obtain a gelatin solution with 1,25% (v/v) of MA. After adding MA, the solution was left to react for an hour and then transferred to conical Falcon tubes for centrifugation at 1200 rpm for 3 minutes. Supernatant was decanted into a glass beaker and the reaction was finally stopped by adding fourth times the initial volume of PBS. Afterwards, GelMA solution was transferred into SnakeSkin Dialysis Tubing 3500 Da (ThermoScientific) and dialyzed against Milli-Q water at 40 °C. Water was changed every 4 hours for three times a day and for three days. Then, the solution was collected and 30 mL were transferred in 50 mL conical Falcon tubes with holes in the lid, covered with parafilm, and left overnight at -80°C. On the next day, the tape was removed from the lids and the solution was lyophilized (Freeze Dryer Alpha 1-4 LD Christ) for 5 days (figure 10-b). Lyophilized GelMA was stored with parafilm at -20 °C.

2.1.2 AlgMA synthesis

A similar process was used to fabricate alginate methacrylate (AlgMA), following a method previously described [38], [54].
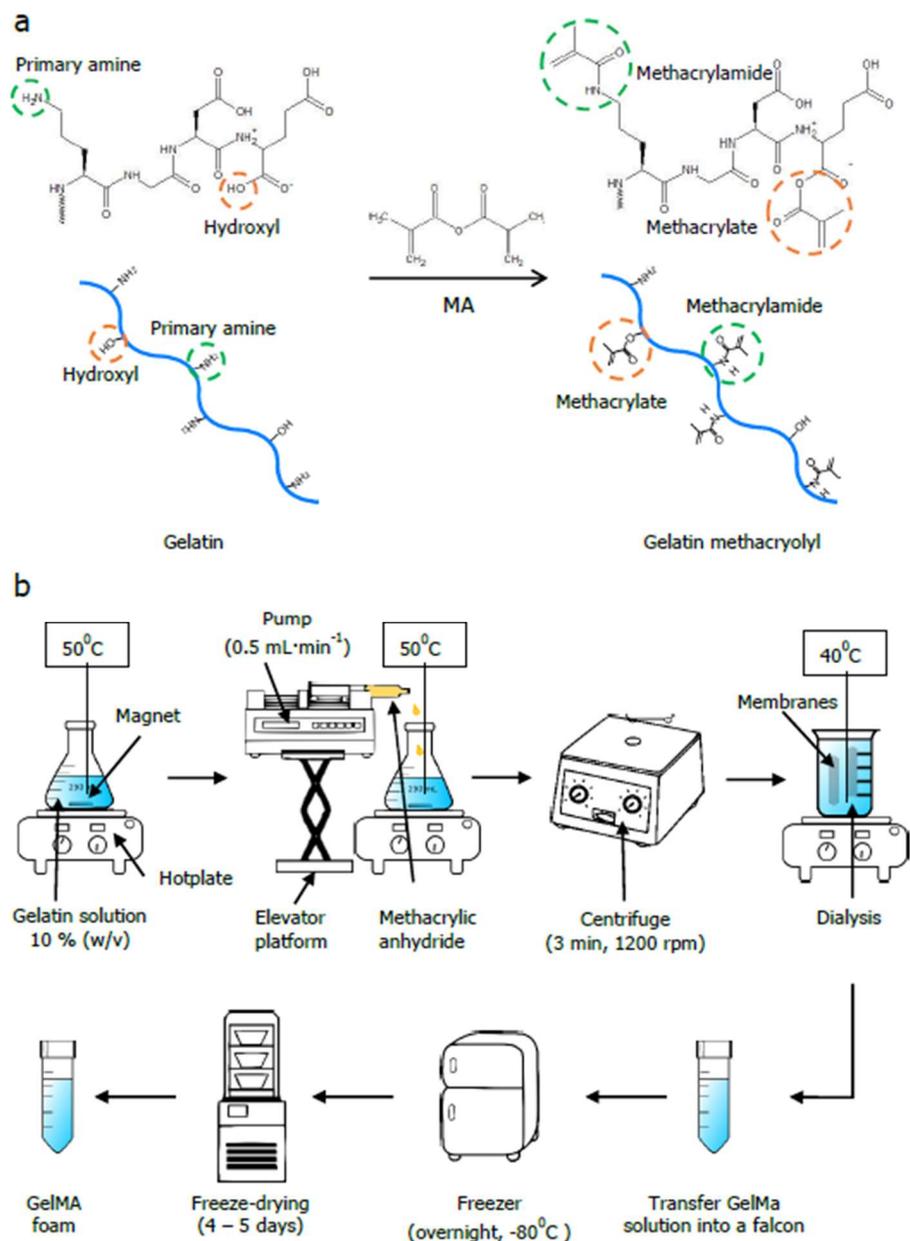
Figure 10. Schematic illustration of the A) reaction of methacrylic anhydride (MA) with the primary amine and hydroxyl groups on the gelatin for the synthesis of gelatin methacryloyl (GelMA) and B) the main steps for GelMA synthesis. Reprinted from [9].

A solution of 1 % w/v of Sodium alginate (Alg) (W201502, Sigma-Aldrich) in 50 mM 2-(N-Morpholino) ethanesulfonic acid (MES) (M2933, Sigma-Aldrich) buffer was mixed at pH 6.5 with 10 mM N-hydroxysuccinimide (130672, Aldrich), 20 mM N-(3- Dimethylaminopropyl)-N-ethylcarbodiimide hydrochloride) (EDC) (03450, Sigma Aldrich) and 10 mM 2-aminoethylmethacrylate (516155, Sigma-Aldrich). The solution was left overnight under vigorous stirring at 40°C. Afterwards, alginate was precipitated with acetone, filtered using a vacuum flask, and dissolved in Milli-Q water. The solution was filtered and dialyzed against deionized water using 3500 Da dialysis skins and kept for a week under constant agitation.

Eventually, the solution was lyophilized for four days to generate a porous dry foam stored at -20°C.

2.2 Determination of the degree of functionalization by H-NMR

Unmodified alginate and gelatin, AlgMA and GelMA were dissolved in deuterium oxide (D_2O) at 65 °C for 1 hour under stirring conditions to estimate the degree of functionalization of the polymers. Then, keeping the temperature at 37 °C, H-NMR spectra were acquired with a spectrometer (Varian INOVA 500 MHz, INOVA). Afterwards, data were collected and analysed with MestReC software (Mestrelab Research). Few adjustments were applied for a proper spectra interpretation. Phase and baseline were tuned, and the chemical shift for GelMA and gelatin spectra was adjusted to the residual solvent signal (D_2O $\delta(1H)$ =4.8 ppm). In the GelMA sample, the DoF quantification depends on the modification of the primary amine groups from Hydroxylysine (Hyl) and Lysine (Lys) aminoacids [55]. Consequently, methacrylation degree was calculated by the rate of the integral of Lys (Lys chemical shift = 3.5-3.4 ppm) of the pure gelatin with the integral of Lys of the GelMA polymer, following the equation (1):

$$DoF\ (\%) = \left(1 - \frac{\int Lysine\ GelMA}{\int Lysine\ Gelatin}\right) * 100 \quad (1)$$

Concerning AlgMA polymers, DoF was calculated following the equations (2-3), where Ha, Hb, H_{M-1}, H_{G-1} represent the integral under the curve of the two vinyl hydrogens in the methacrylate group (Ha and Hb, about 6.1 and 5.7 ppm), the anomeric carbon hydrogen in the mannuronic units (H_{M-1}, about 4.4 ppm) and the anomeric carbon hydrogen in the guluronic units (H_{G-1} about 5.0 ppm) [56][57].

$$G\ (\%) = \frac{H_{G-1}}{H_{G-1} + H_{M-1}} * 100 \quad (2)$$

$$DoF\ (\%) = \frac{\frac{Ha + Hb}{2}}{H_{G-1}} * G \quad (3)$$

2.3 Fabrication of GelMA-AlgMA hydrogel co-network

The final goal was to obtain two different substrates to subsequently analyse differences and similarities felt by fibroblast. First, GelMA-AlgMA hydrogels were fabricated with, on the top, a monolayer of cells. Then, 3D cell-laden hydrogels were prepared.

The system used to cross-link the hydrogels was composed of a silanized glass slide and a circular PDMS mould with a thickness of 250 μm.

Silanization is a method for coating the surfaces of materials such as glass or ceramics. Thanks to the interaction between the hydroxyl groups on the glass and the alkoxy ones on the silane, silanization creates a siloxane bond and develops a silane monolayer on the substrate (figure 11). Then, methacrylate groups of silane react with methacryloyl groups of GelMA and AlgMA. This bond avoids hydrogel detaching from the substrate in an aqueous solution for a long time. Briefly, glass slides were laid into a Petri dish and irradiated for 15 minutes with UV (UV ozone cleaner, Bioforce Nanosciences) to activate their surfaces. Then, the silane solution was added to the Petri dish and incubated for 90 minutes under shaking conditions at 50 rpm and room temperature. The silane solution consists of 3% (v/v) diluted acetic acid and 2% (v/v) 3-(Trimethoxysilyl)propryl methacrylate (TMSPMA) (Sigma-Aldrich) in absolute ethanol (131086, Panreac). The diluted acetic acid solution was prepared 1:10 (v/v) between acetic acid (131008, Panreac) and Milli-Q water. After incubation, the substrates were carefully rinsed with ethanol at 96% (v/v) and dried in the oven at 65 °C for 30 minutes. Glass coverslips were stored in a sealed chamber until use for up a month.
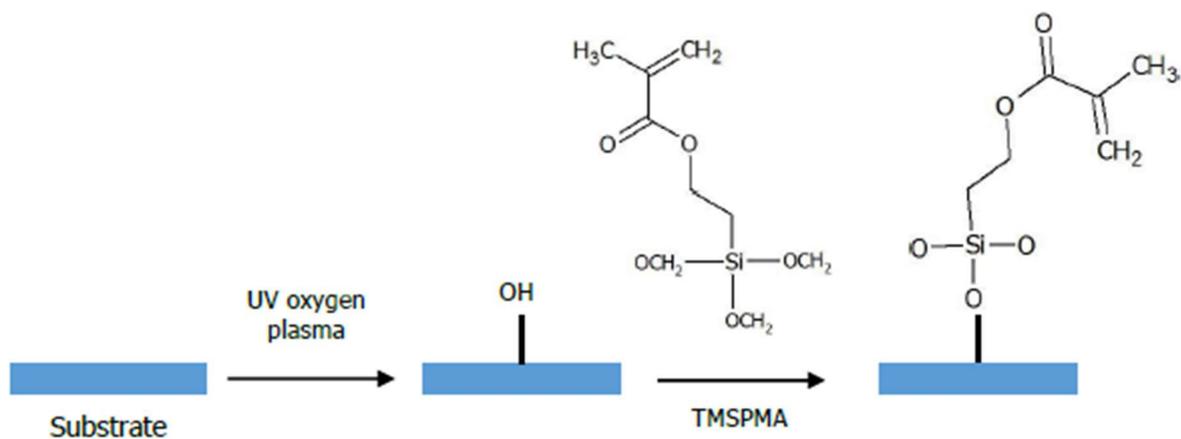
Figure 11. Schematic representation of the silanization process. The hydroxyl – UV activated surface reat silane TMSPMA to silanize the substrate. Reprinted from [9].

23

SYLGARD(R) 184 Silicone elastomer kit (DCE-1673921, Dow Corning) at a 10:1 ratio in the mass of pre-polymer to curing agent was employed to fabricate supports with pools having a diameter of 12 mm and a thickness of 250 μm. Briefly, after mixing the agents gently, they were degassed under vacuum for at least 30 minutes. Therefore, the solution was poured between two flat poly(methyl methacrylated) (PMMA) discs separated by a spacer of 250 μm thick. A weight was placed on top of the PMMA piece, and polydimethylsiloxane (PDMS) was cured at room temperature. After 72 h, PMMA discs were removed, and the thin sheet of PDMS was punched with a circular punch of 12 mm in diameter. The pools have the scope to contain hydrogels polymer solution in order to obtain hydrogels completely flat and with a specific thickness.

Afterwardss, to obtain a final GelMA – AlgMA hydrogel co-network, 5 % w/v of GelMA and 1 % w/v of AlgMA were weighted and sterilized with UV for 15 minutes. Then, the polymers were mixed with high-glucose Dulbecco's Modified Eagle's Medium (DMEM) (Invitrogen) in an amount equal to 90 % of the final volume wanted, put in 15 mL falcon and leave it overnight to dissolve in a water bath at 45 °C. On the next day, the LAP photoinitiator (L0290, TCI) was weighted in a 0.5 % w/v concentration for a stock solution and sterilized with UV for 15 minutes. The stock solution was further dissolved at 1:10 in the GelMA-AlgMA solution to obtain a final LAP concentration of 0.05 % w/v. The solution was carefully pipetted to mix it, avoiding bubbles.

The solution was kept at 40 °C to avoid the solidification of the gel, the moulds were warmed at 37°C in order to simplify the flow of the solution, and 80 μL were pipetted thoroughly between the mould and the silanized glass slide, thanks to a narrow channel. The surplus solution was removed from the channel.

Hydrogels were exposed to UV light using a 3D bioprinter (3DDiscovery BioSafety, regenHU, Switzerland; 365 nm, 3 W·cm^{-2}) for 5 s. Culture medium was rapidly added to the samples.

In conclusion, cells were seeded with the desired concentration ($5 \cdot 10^4$ cells·cm^{-2}) on the top of the hydrogels (figure 12-a).

Conversely, in the case of cell-laden hydrogels, cells were detached with 0.25% trypsin-EDTA, centrifugated at 500 rcf, resuspended to obtain a concentration of 5 million cells, centrifugated another time. Finally, 1 mL of the polymer solution was carefully mixed with the pellet (concentration of 5 million cells per 1 mL of solution). The solution was then added

into PDMS pools and cross-linked with UV as previously described (figure 12-b).
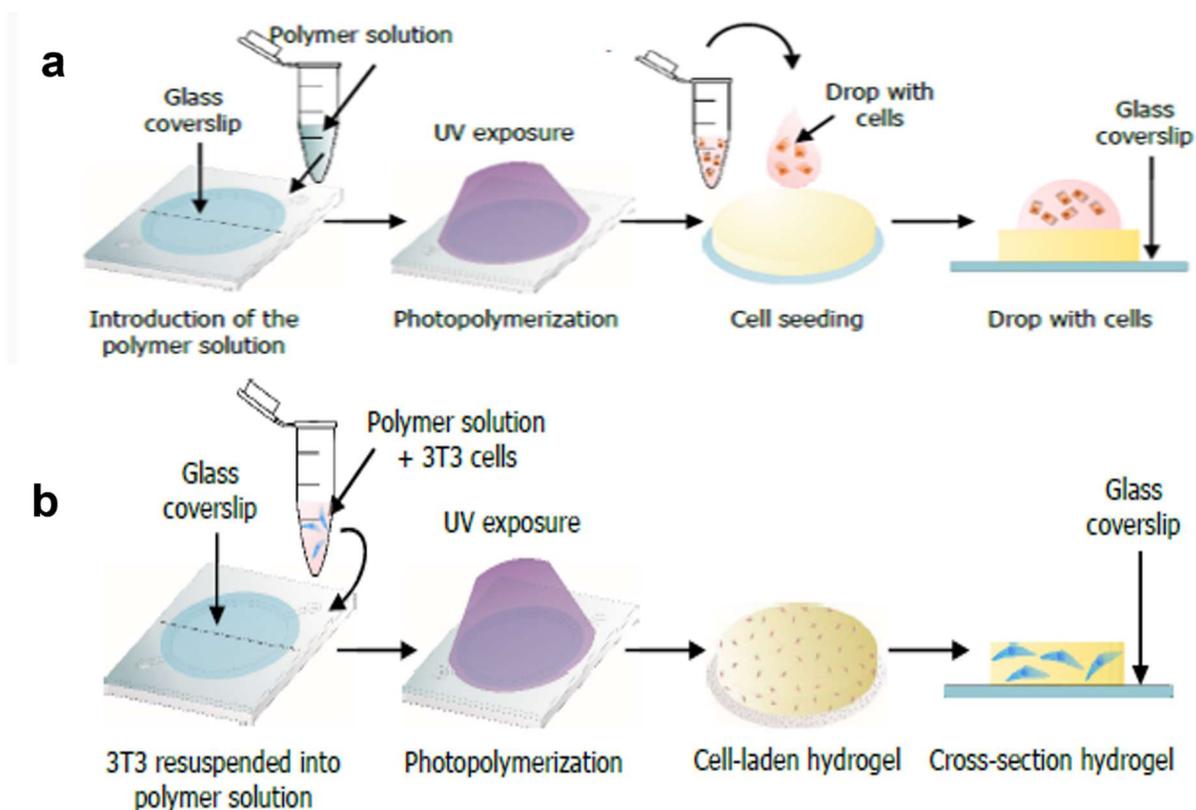
Figure 12. Representation of the hydrogel fabrication process. Polymer solution was poured into PDMS pools covered by a silanized glass slide by a narrow inlet channel and then, photopolymerized. On the top production of hydrogels with a monolayer of cells is shown (a). In the bottom image, cell-laden hydrogel fabrication is represented (b). Reprinted from [9].

2.4 Degradation test

Three drops of 80 µl of the pre-polymer solution were photo-crosslinked and left in a 12-well plate with PBS for three days. Afterwards, samples were filled with a solution of collagenase type II (17101015, Life Technologies) dissolved in PBS at a concentration of 1.5 U·ml⁻¹, and incubated at 37 °C under 100 rpm shaking conditions. Replicas were weighted at different time points (15, 30, 45 min, 1, 2, 4, 6 h). The percentage of hydrogel remaining at each time point was calculated, following the equation (4)

$$W_r(\%) = \frac{W_t}{W_i} \cdot 100 \quad (4)$$

In this equation, W_t represents the mass at a precise time point, and W_i is the initial weight of the replica after fabrication.

2.5 Swelling Analysis

As described above, three drops of 80 μl were prepared for the test on the same day. They were weighed before starting the analysis, kept in dry conditions. Next, PBS was added, and they were weighed again at specific time points (15, 30, 45 min, 1, 2, 4, 6, 8, 24 h). Following equation (5), the swelling ratio was evaluated:

$$\Delta W = \frac{W_s - W_i}{Wi} \cdot 100 \quad (5)$$

In this equation, W_i corresponds to the initial weight of the replica after fabrication, W_s is the weight after swelling. To normalize the value, the mass increment was divided by the initial weight.

2.6 Mechanical characterization of GelMA-AlgMA hydrogels

It is fundamental to know the mechanical properties of the fabricated hydrogel because they highly influence how cells behave. Hence, the mechanical properties of the GelMA-AlgMA hydrogels were investigated.

2.6.1 Compression test

First, dynamic mechanical analysis (DMA) was performed. This technique characterizes the mechanical properties of bulk hydrogels [9]. GelMA – AlgMA hydrogels co-network (concentration of 5 % w/v and 1 % w/v) were fabricated with a cylindrical shape of 6 mm in diameter and 3 mm in height thanks to Teflon moulds. The energy dose used was 15 J·cm^{-2}. For statistics, five hydrogels of each condition were inspected.

After photopolymerization, the hydrogels were detached, and the diameter recalculated. The compression test was performed with a Zwick-Roell Zwichi Z0.5TN testing machine (Zwick Roell Group) (figure 13-a), and force–deformation curves and data were obtained at room temperature. PBS drops were put onto the samples to ensure hydrogel hydration during the test.

Force-deformation data were obtained applying a pre-load of 0.5 mN, a limiting strain rate of 10 % min^{-1} and a maximum strain of 30 %. Row data were analysed and plotted with OriginPro 2019b (OriginLab, USA). The elastic modulus (E) was evaluated from the slope of the linear region of the stress-strain plot, corresponding to a strain range of 10 % - 20 % (figure 13-c).
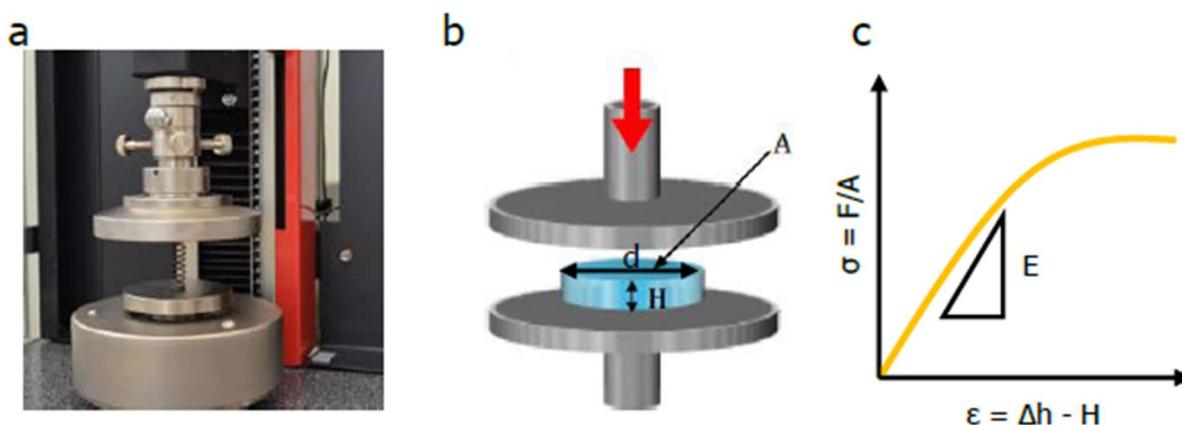
Figure 13. Compression test. A) photograph of the Zwick-Roell Zwicki machine employed. B) Schematic illustration of the compression test and C) representation of stress (σ)-strain (ε) curve to compute the Young's modulus. Reprinted from [9].

2.6.2 Rheological analysis

To further investigate the mechanical properties of the hydrogel sensed by cells, a rheological characterization was performed on an Anton Paar (MCR 702) rheometer (figure 14).

The controlled shear rate (CSR) test investigates the complex non-Newtonian behaviour of materials and is used when viscosity should be measured at a specific shear rate. Frequency sweeps test is a characterization performed at variable frequencies and a constant amplitude aiming to investigate time-dependent deformation behaviour. Amplitude sweep (or strain sweep) is a test performed at constant frequencies and variable amplitudes that analyse storage and loss moduli [58].

The measurements were carried out using a configuration of a plate-cone geometry, using 39,95 mm the plate diameter and 1,005 º the cone angle and a gap of 78 µm. Drops of 500 µl were photo-crosslinked, and the test was performed at a constant temperature of 37 °C.

Frequency sweep test settings were an angular frequency from 0.1 to 100 rad·s^{-1} and a strain of 0.1 %, amplitude strain sweep settings were frequency equal to 1 Hz, strain from 0.01 to 100 %, and CSR had a shear rate ramp of 0-100 s^{-1}.

Figure 14. Photograph of the Anton Paar (MCR 702) rheometer.

Furthermore, CSR tests were carried out at different temperatures to evaluate the material's printability for future work development (5, 10, 15, 20, 21, 22, 23, 24, 25 °C). These tests were performed on the solution before being cross-linked.

All the row data were analysed and plotted with OriginPro 2019b (OriginLab, USA).

2.7 Gelatin coating

The third type of substrate was assessed in the comparison between substrates.

Microscope glass slides (Ø 18 mm, Superior Marienfeld) were cleaned with soap and water, dried with N$_2$ and disinfected with 70% ethanol and UV for 15 minutes. Next, they were incubated with a 1% sterile gelatin solution from porcine skin in Milli-Q water for 1 h at 37 °C, rinsed twice with PBS, and cross-linked with a solution of 1 % filtered glutaraldehyde (G6257, Sigma) in PBS for 20 min at room temperature. After washing twice with PBS, the

reaction was quenched with 1 M sterile glycine Bioultra (50046, Sigma-Aldrich) PBS solution for 30 min at room temperature, and glass slides were lastly washed with PBS. The coated coverslips were used immediately or stored in the fridge with PBS and 1 % Penicillin and Streptomycin (15140122, Invitrogen) for a maximum of two weeks.

Afterwards, 1 mL of medium containing $5 \cdot 10^4$ cells·cm^{-2} of fibroblasts were added to the gelatin substrate.

2.8 Cell culture

Commercial NIH-3T3 mouse fibroblasts (ATCC) and NIH-3T3 secreting fluorescent fibronectin were used. NIH-3T3, genetically modified to secrete fibronectin (FN) labelled with the fluorescent molecule Ypet, were kindly gifted by Prof. Riveline (Laboratory of Cell Physics, University of Strasburg) [59].

NIH-3T3 and NIH-3T3 Ypet-FN were grown in high-glucose Dulbecco's Modified Eagle's Medium (DMEM) (41965039, Invitrogen) supplemented with 1 % Penicillin and Streptomycin (Invitrogen), 1 % Sodium Pyruvate (11360039, Sigma-Aldrich) and 10 % Fetal Bovine Serum (10270106, Gibco), at 37 °C and 5% CO_2. For the subculture of modified fibroblasts, G418 antibiotic was added to the culture media to select cells encoding FN-Ypet. Cells were cultured in T-75 flasks and harvested at 80% confluency with 0.25% trypsin-EDTA (25200056, Life Technologies) for 5 minutes.

2.9 CDMs deposition

The protocol for cell-derived matrices (figure 15) deposition was adapted from existing
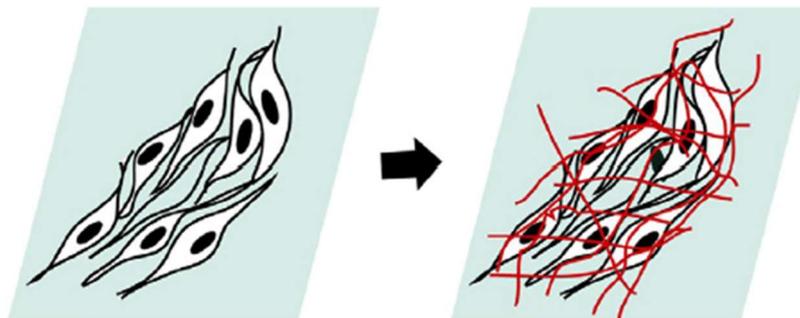
Figure 15. Schematic representation of CDM production. In red, the extracellular matrix generated. Reprinted from [59].

methods [10], [16]. Two days after seeding, L-Ascorbic acid (A.A.) (95209, Sigma-Aldrich) treatment was started. Standard culture media supplemented with 50 µg·mL^{-1} A.A. was added every two days for eight days to stimulate collagen generation and stabilize the generated matrix. Samples were monitored using brightfield microscopy (Olympus IX71).

2.10 Cells distribution and secretion

In order to evaluate cell distribution and secretion on the different substrates, a staining with Phalloidin-iFluor 594 Reagent (ab176757, Abcam) and Hoechst 33342 (H3570, Life Technologies) was performed. Hoechst is excited by ultraviolet light and emits an intense blue fluorescence at a wavelength of 460-490 nm [60]. Phalloidin-iFluor 594 is one of many phalloidin conjugates: it has an excitation wavelength of 590 nm and an emission one of 618 nm. [61]

Samples were washed twice with PBS and fixed for 20 minutes with Formaldehyde solution (1:10 in PBS) (252549, Sigma) and then washed again. Phalloidin and Hoechst were diluted 1:1000 in PBS, and 1 ml of the solution was added for each sample for 30 minutes and room temperature. Finally, samples were washed again in PBS and stored with 1 % sodium azide (71290, Sigma) in PBS in the fridge. They were analysed using a confocal laser scanning microscope (Leica TCS SP5MP System) as described below.

2.11 Viability assay

The viability of NIH-3T3 cells embedded in GelMA 5%-AlgMA 1% hydrogel was assessed using a Live/Dead assay kit (L3224, Termofisher) containing Calcein AM (4mM) and Ethidium homodimer-1 (Eth-D1). Intracellular esterase enzyme in alive cells converts the non-fluorescent Calcein molecule to an intensely fluorescent Calcein that produces green fluorescence. Therefore, Calcein is kept inside cells and produces fluorescence at 494/517 nm excitation/emission wavelengths. Eth-D1 is a cell membrane-impermeable substance able to penetrate only broken membranes. Then, it binds to the DNA of dead cells: this interaction changes the conformation of Eth-D1 that produces red-fluorescence at 528/617 nm (figure 16) [62].

Hoechst (H3570, Life Technologies) was added to stain cells nuclei.

A solution of 1 % v/v Hoechst, 1,5 % v/v of Calcein, 1,5 % v/v of Eth-D1 in DMEM was prepared. Hydrogels were washed three times with PBS, and 1 ml of solution was added for each sample. Cells were incubated for 1 hour at 37 °C, 5% CO_2 and then washed again with PBS at least three times. Samples were covered with foil. This assay was performed on day one and day eight, and, for statistical analysis, three samples were stained for each day.

Samples were imaged using a confocal laser scanning microscope (Leica TCS SP5MP System) as described below.
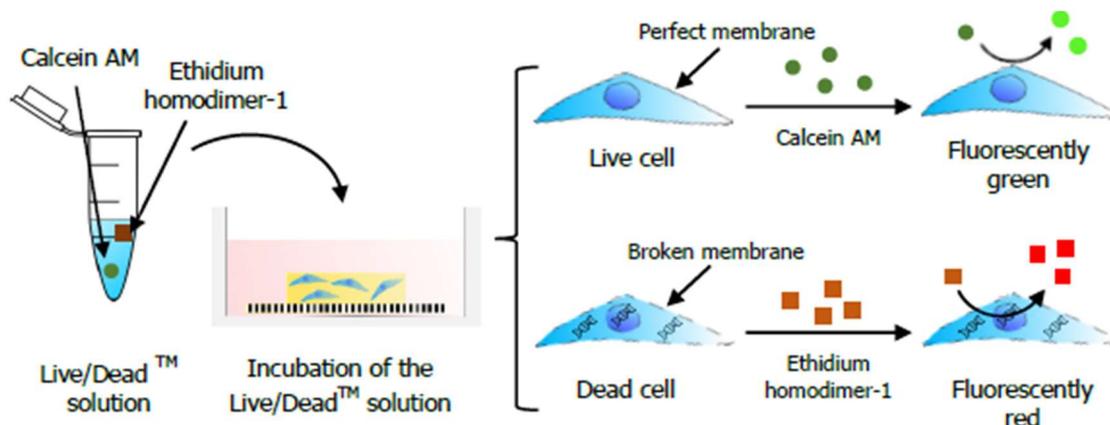
Figure 156. Illustration of Live/Dead viability assay. The kit contains calcein AM and ethidium homodimer-1. The first one is modified by intracellular esterases of the live cells to give a green fluorescence emission. The second one interacts with the DNA of the dead cells showing a red fluorescence emission. Reprinted from [9].

Finally, images were segmented through KNIME analytic platform and viability was computed as:

$$Viability\ (\%) = \frac{N°\ Alive\ cells}{N°Alive\ cells\ +\ N°\ dead\ cells} * 100 \quad (6)$$

2.12 Confocal Microscopy

Confocal laser scanning microscopy (Leica TCS SP5MP System, 20x air or 40x oil objectives, NA 0.75 and 1.4 respectively) was employed to collect immunofluorescence images. The 3-dimensionality of hydrogels was reconstructed with several z-stacks separated 5 µm from each other. The power of the lasers and the gain of the detector were maintained constant across samples.

2.13 Image Analysis

Image analysis was performed with Fiji and KNIME (University of Konstanz, Zurich, Switzerland) analytic platforms. Briefly, confocal images were uploaded to the software and brightness and contrast were adjusted for each channel (brightfield, blue, green and red). After blurring images with a Gaussian filter, multiple z-stacks were projected to a single image with the option of maximum intensity. Next, each colour channel was analysed separately: global threshold (method: Yen [63], [64]), fill holes and watershed tools were applied. Regions with an area smaller than 17.5 pixel^2 were eliminated, and the number of nuclei, alive and dead cells was calculated (figure 17).

2.14 Statistical Analysis

All data were plotted with Origin (Pro) (Version 2019b, OriginLab Corporation, Northampton, MA, USA) and presented by the mean ± standard deviation. For viability studies, statistical analysis was performed using Oneway ANOVA. P-values higher than 0.05 were considered non-significant.
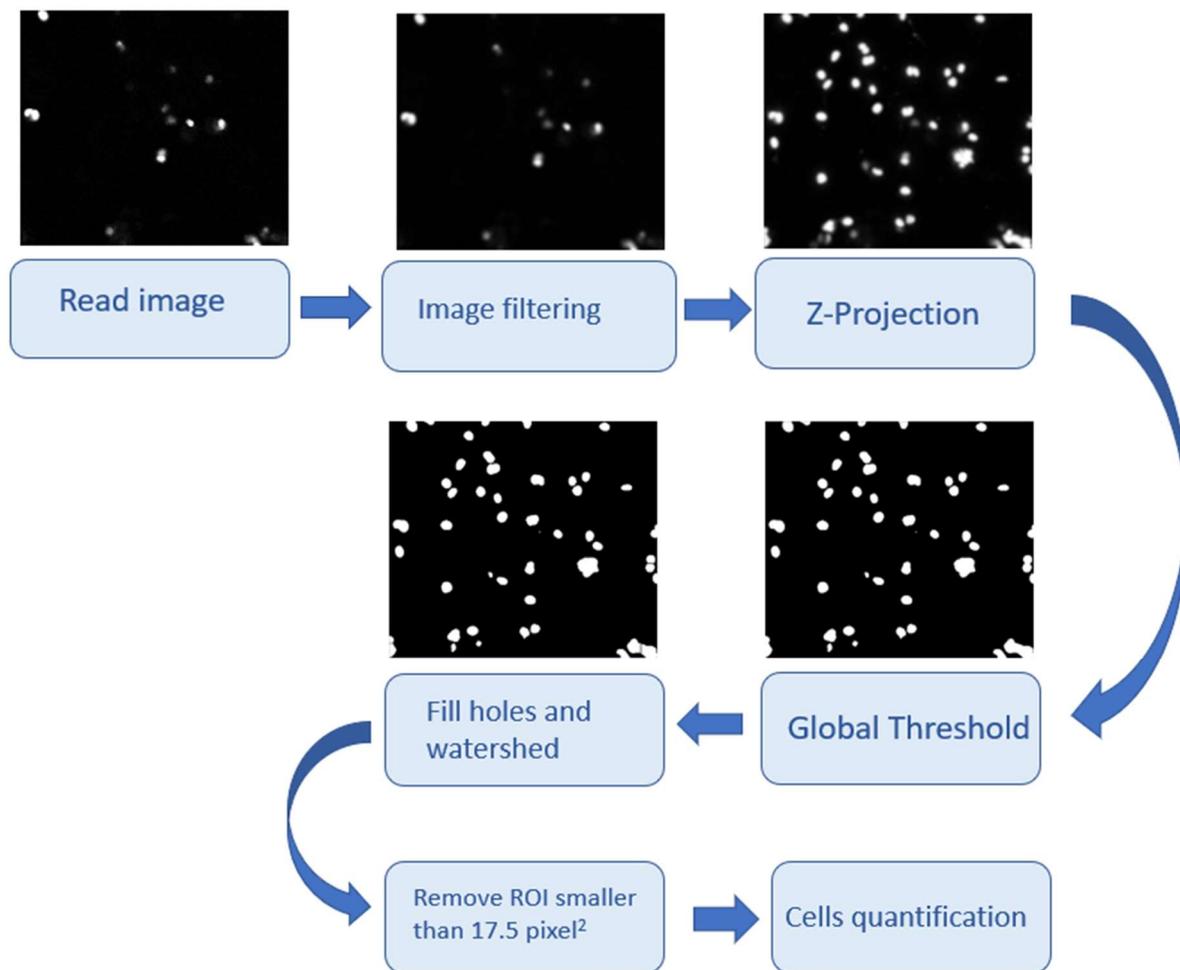
Figure 167. Scheme of the image analysis process

3 Results

Firstly, an accurate literature study about gelatin properties related to different parameters was carried out. Gelatin was the selected biopolymer for its high biocompatibility and bioactivity. Table 1 summarises several works that have been studying the influence of many factors in tailoring the mechanical, diffusion and degradation properties. As it can be seen, a wide range of compressive modulus can be achieved, mainly increasing the degree of functionalization, the percentage of GelMA and photoinitiator, and the UV power and exposure time. Likewise, long-lasting hydrogels can be produced by increasing these parameters and, overall, excellent properties can be reached. However, increasing these variables dramatically increases the hydrogels' toxicity, as reported elsewhere, resulting in an impractical strategy. For this reason, numerous works have put effort into studying this material combined with other biopolymers. Following this path, alginate methacrylate was added. Indeed, it is well-known that AlgMA can improve the mechanical properties of GelMA hydrogel, rising stiffness, durability and improving water take.

3.1 Determination of the degree of functionalization by H-NMR

Firstly, gelatin methacryloyl (GelMA) and alginate methacrylate (AlgMA) were prepared following a method previously described, and the proper synthesis of GelMA and AlgMA was verified. The degree of functionalization (DoF) was evaluated because it is an essential parameter to guarantee the reproducibility of synthesis procedures. Proton nuclear magnetic resonance (H-NMR) was performed to qualitatively assess the synthesised polymers' methacrylation and study the DoF.

% v/v MA	DoF	% w/v GelMA	Photo initiator	% w/v photo initiator	UV time	UV power or dose	Compressive Modulus	Eventual copolymer analysed for improving hygrogels properties	Type of cells	Aim of the work	Ref.
1.25 %	40 %	5 % 1 %	LAP I2959	0.1 % 0.4 %	5 s 25 s	P = 3 W/cm²	3.02 ± 1.13 kPa	CMCMA AlgMA PEGDA	C2C12 Myoblasts	Give structure and support myotube formation and alignment	[38]
5 % 20% 1.25 % 0.25 %	75 % 78% 50 % -	7.5 % 12.5 %	I2959	0.5 %	-	Dose = 1.5 J/cm²	13.2±0.2 kPa 49.70±3.98 kPa	PEGDA	NIH 3T3 fibroblast	To develop and characterize hydrogels that emulate the in vivo lamina propria features in terms of mechanical and physicochemical properties	[9]
20 % 0.25% 1.25%	81.4 ± 0.4 19.7 ± 0.7 53.8 ± 0.5	5 % 10 % 15 %	I2959	0.5 %	15 s	P = 6.9 mW/cm² Dose = 103.5 mJ/cm²	≈ 3.5 kPa	-	NIH 3T3 fibroblasts	To create cell-laden microtissues and microfluidic devices	[39]
20 %	-	5 % 10 % 15 %	LAP	0.05 %	12 s	-	46.78 kPa ≈ 70 kPa 82.05 kPa	-	NPCs	To evaluate the encapsulation of NPCs in a photosensitive hydrogel made of collagen hydrolysate gelatin and methacrylate (GelMA) to improve NP regeneration	[35]
11.11 % 2.22 % 0.44 %	91.7 ± 1.4 52.5 ± 1.2 25.8 ± 0.7	10 %	I2959	0.5 %	120 s	-	29.9 ± 3.4 kPa 17.1 ± 2.4 kPa 3.8 ± 0.3 kPa	-	Chondrocytes	To study the influence of hydrogel stiffness on chondrocyte phenotype while excluding the role of biochemical factors, such as adhesion site density in the hydrogels.	[65]
-	-	10 %	I2959	0.5%	15 s 30 s	P = 6.9 mW/cm²	≈ 5 kPa (15 s) ≈ 11 kPa (30 s)	-	NIH 3T3	Direct-write bioprinting of a cell-laden photolabile ECM-derived hydrogel	[36]
20 %	-	3%	I2959	0.5 %	15s 25s 40 s	P = 6.9 mW/cm²	0.68 ± 0.02 kPa 1.23 ± 0.11 kPa 2.03 ± 0.09 kPa	-	iNSCs	GelMA was used to photoencapsulate iPSC-derived neural stem cells (iNSCs) and provided an excellent scaffold material for SCI repair.	[41]
-	82-85 %	5 % 10 % 15 %	I2959	0.5 %	90 s	P = 10 mW/cm²	49.9 ± 5.7 kPa 78.7 ± 7.0 kPa 139.1 ± 8.6 kPa	-	hDF	To show the feasibility of GelMa in skin tissue engineering and its potential as an alternative for skin transplants	[42]

Table 1. Summary of several works that have been studying the influence of many factors in tailoring the mechanical, diffusion and degradation properties of GelMA hydrogels.

3.1.1 Gelatin methacryloyl

H-NMR spectra of pure gelatin and GeLMA is represented in figure 18. As it can be noticed, GelMA and gelatin spectra are rather different. Due to the reaction between MA with amine groups (-NH₂) of hydroxylysines (Hyl) or lysines (Lys), three different peaks appear in the GelMA spectra. These are the results of adding methacryloyl groups in the gelatin chain [55], [40]. Recent studies have shown that when there is an excess of MA, it reacts with the hydroxyl groups (-OH) of aminoacid residues. The methacryloyl groups attached to the –NH₂ are known as methacrylamide groups, while the methacryloyl groups attached to the –OH are known as methacrylate groups [40],[55]. Therefore, the name given to modified gelatin is gelatin methacryloyl to includes the two modifications. The three signals that appear in the GelMA spectra correspond to the acrylic protons incorporated into the lysine or hydroxylysine residues (6.2 and 5.9 ppm respectively, figure 18, red square, A) and to methyl protons of the new methacryloyl groups incorporated into the lysine, hydroxylysine residues
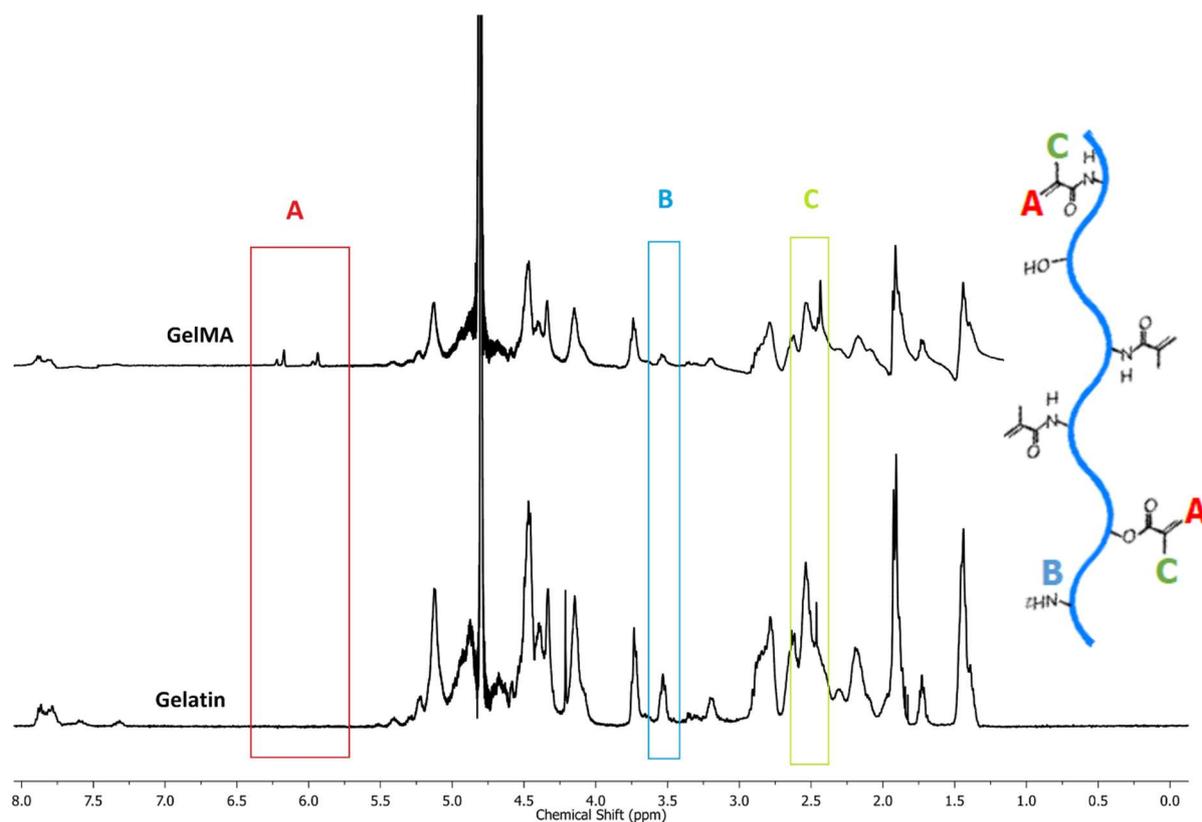
Figure 18. H-NMR spectra of GelMA (top) and gelatin (bottom). In the spectra, bands appear at 5.9 and 6.2 ppm (red square, A), corresponding to the acrylic protons incorporated into the lysin and hydroxylysine residues. At 3.5 ppm (blue square, B), the peak's disappearance is due to the decrease of amino groups from the modified lysin and hydroxylysine. The band at 2.5 ppm (green square, C) represents the methyl protons from the methacryloyl groups. On the right, there is a schematic representation of the GelMA molecule that indicates the bands of the H-NMR spectra [9].

or hydroxyl groups (about 2.5 ppm, figure 18, green square, C). Conversely, the peak at 3.5 ppm (figure 18, blue square, B) diminishes in GelMA spectra because it corresponds to the methylene protons of the free lysine or hydroxylysine residues of the pure gelatin. Overall, the success of the methacrylation process was confirmed.

A comparison in the decrease of peaks of lysines of the GelMA spectra to one of the pure gelatin spectra was performed to establish the degree of functionalization of the GelMA fabricated. Indeed, this method is widely used in the literature [33],[65]. The DoF results from the modification of both primary amine groups and hydroxyl groups, but this method only quantifies the DoF of the methacrylamide groups. However, it is a reasonable estimation because hydroxyl groups are less than 10 % of all the methacryloyl groups [66]. Moreover, when MA is not in surplus, it primarily reacts with free amino groups of lysine and hydroxylysine [67]. The DoF estimated was 46.6 ± 5.9 %, and it agreed with previous works [9], [38].

3.1.2 Alginate methacrylate

Pure alginate (Alg) and alginate methacrylate (AlgMA) spectra are shown in figure 19. The two spectra present distinctive peaks between 3.5 and 5.2 ppm, which stand for the saccharide units of the alginate backbone. Moreover, in the AlgMA spectra can be seen signals at 6.1 and 5.7 ppm corresponding to the vinyl hydrogens of the methacrylate groups (Ha and Hb, figure 19) and at 1.80 ppm corresponding to the methyl hydrogens of the methacrylate groups. The G value had to be calculated as a factor to correct the presence of mannuronic acid.

The G and DoF percentages were calculated from the spectra, and they were 49.98 ± 2.38 and 28.7 ± 3.94, respectively. Results were in agreement with previous studies [38], [56].
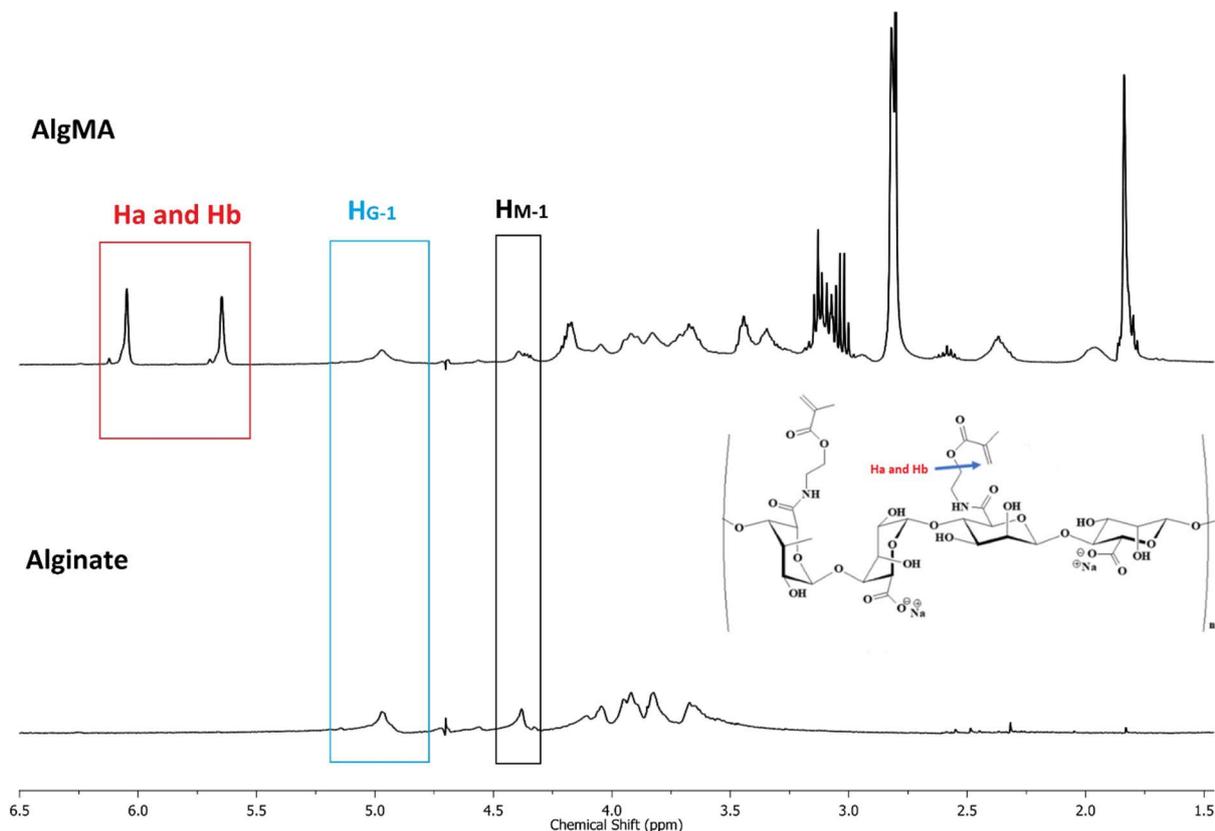
Figure 19. H-NMR spectra of AlgMA (top) and alginate (bottom). In the spectra bands appear at 5.7 and 6.1 (red square, Ha and Hb) corresponding to the vinyl hydrogens of the methacrylate groups. The peak 5.0 ppm corresponds to the anomeric carbon hydrogen in the guluronic units (Blue square, H_{G-1}) and the peak at 4.4 ppm corresponds to the anomeric carbon hydrogen in the mannuronic units (black square, H_{M-1}). On the right, there is a schematic representation of the AlgMA molecule that indicates the bands of the H-NMR spectra [34].

3.2 Stability of the hydrogel co-network

The physical properties of hydrogels, such as swelling ratio and degradation time, are fundamental in evaluating their potential in CDMs production and tissue regeneration. Samples were prepared as previously described to study the ability of the network over time. The photoinitiator chosen was LAP because previous work [38] showed that hydrogels with the same composition but mixed with I2959 were too weak and completely degraded in 1 hour.

3.2.1 Degradation test

A degradation test was performed using collagenase II at a concentration of 1.5 U·ml^{-1}. Collagenase is a protease intended for cell disaggregation. It has specificity for the amino acid (X) and glycine bond in Pro-X-Gly-Pro sequences, present in collagen [68].

Samples were left swelling for three days and then incubated with a collagenase solution. After six hours, the mass remaining was 74 % (figure 20), and this result is in agreement with previous studies [38]. Indeed, gelatin is a collagen derivate, and the enzymatic activity degrades this component. In particular, it exhibits sequences recognized by metalloproteinases, responsible for degrading collagen, laminin, fibronectin, among others [69]. The MMPs responsible for gelatin degradation are MMP-2 and MMP-9, which are
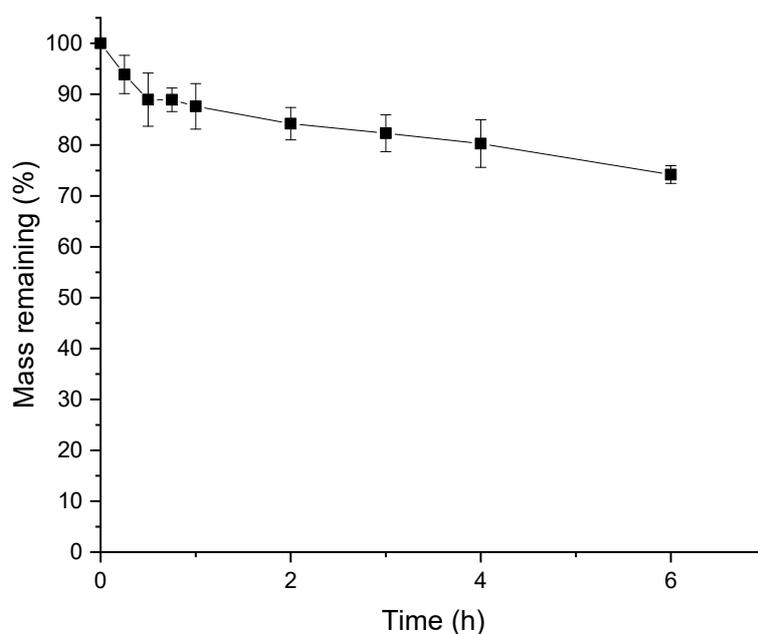
Figure 20. Percentage of polymer mass remaining during the incubation with Collagenasa type II. (mean ± standard deviation, n = 3)

secreted by cells [70]. Previous studies have demonstrated that cells encapsulated in GelMA hydrogels were able to produce high levels of MMP-2 and MMP-9 [69]. As reported by previous studies, pristine GelMA would be totally degraded within 4 hours. Still, thanks to alginate, the degradation rate was significantly decreased (figure 20). Alginate remains since it is not degradable by mammalian cells and provides stability to the hydrogel co-network [43].

3.2.2 Swelling analysis

Drops of the copolymer were fabricated to study the swelling properties. The swelling ratio is depicted in figure 21. All the samples swelled rapidly in the initial hours, achieving a peak after 8 hours. Then, the curves became flat, and the equilibrium was reached after about 24

hours. The value of the equilibrium swelling obtained is in concordance with a recent publication [71].

Tavafoghi and colleagues have seen that the addition of AlgMA in the gel increases the swelling ratio by more than 15 %. Indeed, an AlgMA-free GelMA hydrogel has a swelling ratio after 4 hours about, approximately, 5 %, that can increase until 20 % mixing GelMA with a 3 % of AlgMA polymer [71]. Therefore, the difference in water uptake is due to the hydrophilic structure of AlgMA. Moreover, the molar extinction coefficient determines the free radicals generated as a function of the irradiating wavelength. The LAP molar extinction has a value of $\varepsilon = 218$ $M^{-1} \cdot cm^{-1}$, which is really high and is one of the reasons for the material's excellent swelling capacity [72].
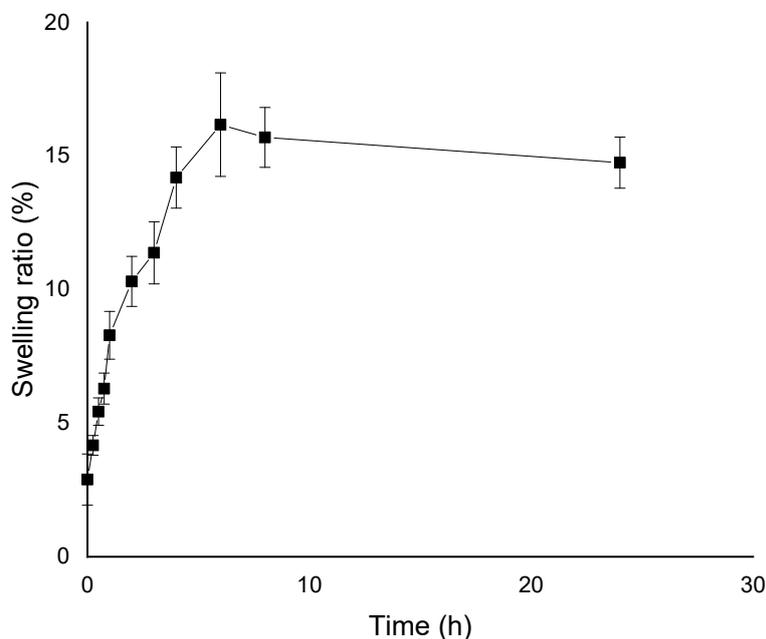
Figure 17. Swelling ratio of the 5 % (w/v) GelMA – 1 % (w/v) AlgMA hydrogel. (mean ± standard deviation, n = 3)

3.3 Mechanical characterization of hydrogel co-network

3.3.1 Compression test

A compression uniaxial mechanical test evaluated the mechanical properties of the biomaterial. A deep study of the GelMA Young's modulus was performed analysing previous works (table 1) before choosing to add a percentage of AlgMA. AlgMA was added mainly to rise compressive modulus and degradation time, two fundamental characteristics for CDMs production purposes.

40

Disc-shaped hydrogels were photopolymerized using the same UV dose as for cells experiments. Two of the five hydrogels tested recorded a failure at around 20 % of strain, probably due to shape and fabrication defects. Still, all the samples present a linear behaviour in the first region of the curves, demonstrating that they behaved as elastomers. Elastic modulus was 0,990 ± 0,239 kPa and was evaluated from the linear part of the curves, ranged from 10 % to 20 % of the total strain. Similar modulus values were reported in the literature. Monferrer *et al.* disclosed values of 1.11 ± 0.12 kPa [73], while in another work, Garcìa-Lizarribar *et al.* have measured a Young modulus of 5.53 ± 2.01 kPa due to a slight increase of the LAP percentage [38]. Comparing with pristine GelMA photocrosslinked with the same conditions (0.28 ± 0.08 kPa [73]), a higher compressive modulus was encountered. Moreover, Garcìa-Lizarribar *et al.* found that GelMA-AlgMA hydrogels have the highest compressive modulus also compared to other composites hydrogels prepared with the same conditions (GelMA - Carboxymethylcellulose Methacrylate, GelMA - Poly(ethylene glycol) diacrylate [38]). Indeed, AlgMA has a secondary ionotropic gelation due to divalent ions such as Ca^{2+} contained in the medium. This specific gelation is responsible for the relevant differences in stiffness compared with other materials [38].

3.3.2 Rheological analysis

The science of deformation and flow is named rheology, a term derived from the Greek *rheos,* which means "to stream" or "to flow" [74]. The primary purpose is to study the response of solid material to deformation and the flow behaviour of liquids. However, only ideal solids deform purely elastically, following the Hook's low, and only ideally viscous liquids flow exclusively. Indeed, the mechanical response of most materials is based on a combination of elastic and viscous behaviour, known as viscoelasticity. However, depending on the timescale of the rheological experiment, all materials can respond as liquid or solid.

Three different tests were carried out to study the specific rheological properties of GelMA-AlgMA hydrogels. In figure 22, the shear rate-dependent behaviour is presented. In Newtonian ideally fluids, the shear stress is linearly related to the shear rate, and hence the viscosity is invariable with the shear rate or shear stress. On the contrary, non-Newtonian fluids are those where the viscosity varies as a function of the applied shear rate or shear stress. In the current case, the behaviour until the shear stress of 1 s^{-1} was Newtonian. Afterwards, the hydrogel behaves as a shear-thinning material, according to a previous study [75]. Without any external load, each macromolecule of the polymer stays in the lowest level of energy consumption, showing a three-dimensional coil shape. Each coil is entangled repeatedly with other close macromolecules. In the shear process, the macromolecules can be or not oriented in shear direction and when under shear process, the molecules disentangle, diminishing their flow resistance. However, when the shear rate is less than 1 s^{-1}, many macromolecules are oriented in the shear direction and can partially disentangle, decreasing viscosity in the volume. Concurrently, other macromolecules are recoiling again thanks to their viscoelastic behaviour, increasing the viscosity again. As a result of the two processes, no significant changes are displayed on the whole volume, showing a constant viscosity typic of Newtonian fluids. Afterwards, increasing the shear rates, the disentanglements exceed the recoil number, and the polymer behaves as shear-thinning [58].
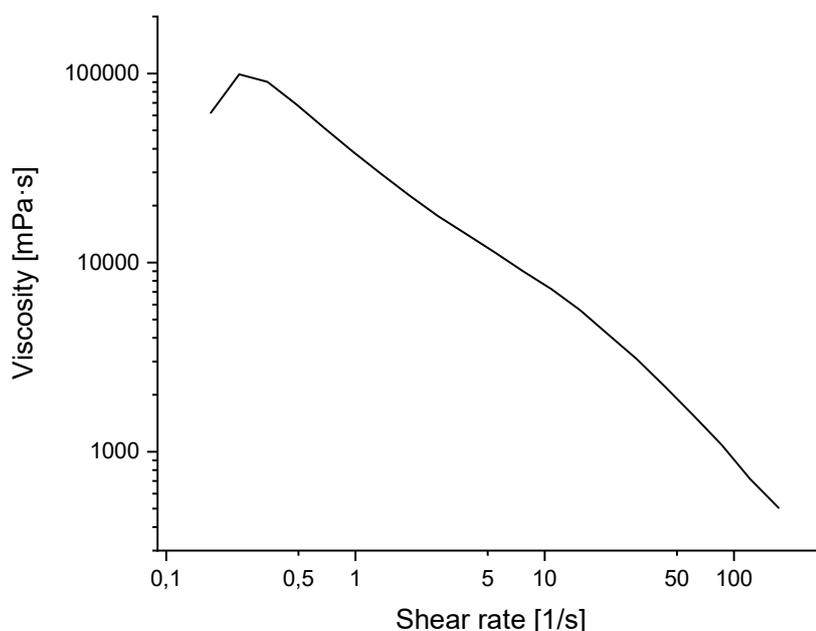
Figure 18. Viscosity versus shear rate for the 5 % (w/v) – 1% hydrogel. Axis in logarithmic scale.

Oscillatory strain experiments have become widely employed in the last fifteen years to analyse the diverse behaviour of materials. Hence, a sinusoidal strain is applied to the sample at a frequency ω using a cone plate geometry. A material completely elastic will have zero phase delay in the stress wave, and, by contrast, a purely viscous material will be 90 ° out-of-phase. More often, the stress will have a phase difference between 0° and 90°. The shear storage modulus G' corresponds to the elastic and in-phase behaviour, while the shear loss modulus G" corresponds to the viscous and out-of-phase one. G' and G" are defined by equation (7), being G* the complex shear modulus and τ^* the complex shear stress:

$$G^* = \frac{\tau^*}{\gamma} = (G'^2 + G''^2)^{1/2} \quad (7)$$

The two oscillatory tests performed were the amplitude sweep test and the frequency sweep test. The amplitude sweep test is carried out at a constant frequency and variable amplitudes. The test was performed with a controlled shear strain: $\gamma(t) = \gamma_A(t) * sin(\omega t)$ (strain amplitude sweep test). As it is possible to observe in figure 23, G' is higher than G", so the elastic behaviour dominates the viscous one. Usually, this test is performed to establish the limit of the linear viscoelastic (LVE) range, considered the maximum permissible strain,
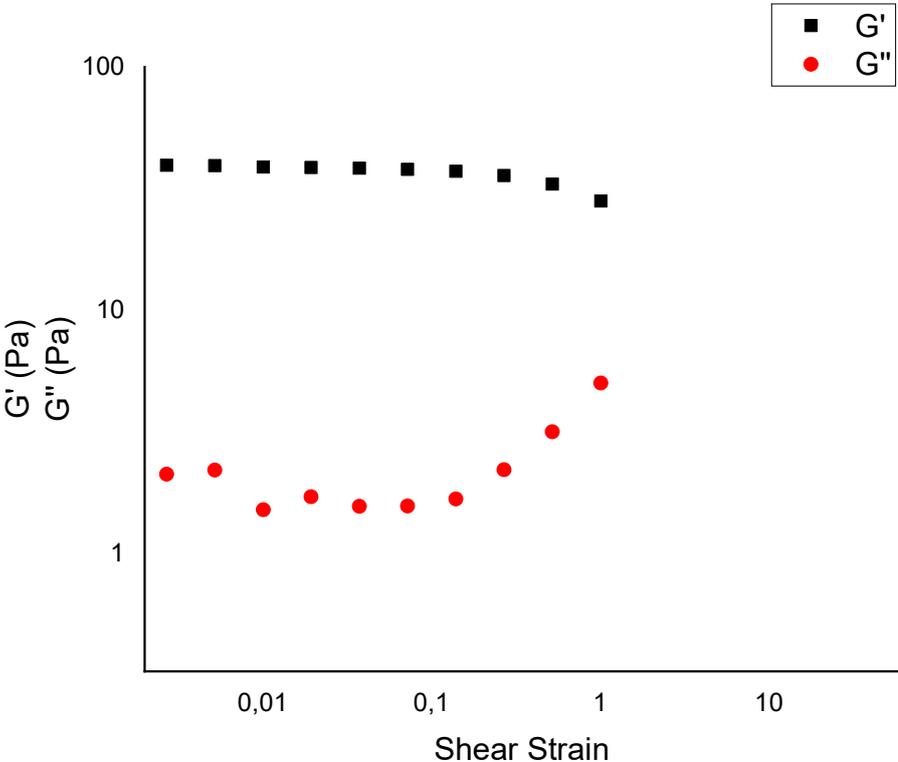
Figure 19 Storage modulus and loss modulus versus oscillatory shear stain (frequency = 1 Hz). Axis in logarithmic scale.

avoiding irreversible structure changing. In this case, the LVE is approximately around 10 % of the shear strain.

Therefore, a shear strain of 0.1 % was chosen to perform the frequency sweep test in an LVE range. This analysis was carried out to investigate time-dependent deformation behaviour and was performed with controlled shear strain: $\gamma(t) = \gamma_A * sin(\omega(t)t)$ (strain frequency test). The curves (figure 24) display a brief slope before reaching the plateau value for both moduli. In the plateau range, the loss factor tanδ = G''/G' is about 0.17. This value represents the ratio of the sol and gel components [58]. The first one is the unlinked part and reflects the mobile molecule chains, while the second one represents how molecule chains integrated into the network behave. In the linear region, the value of G' is about 57 Pa, and G" is around 10 Pa, according to previous studies [76], [77].
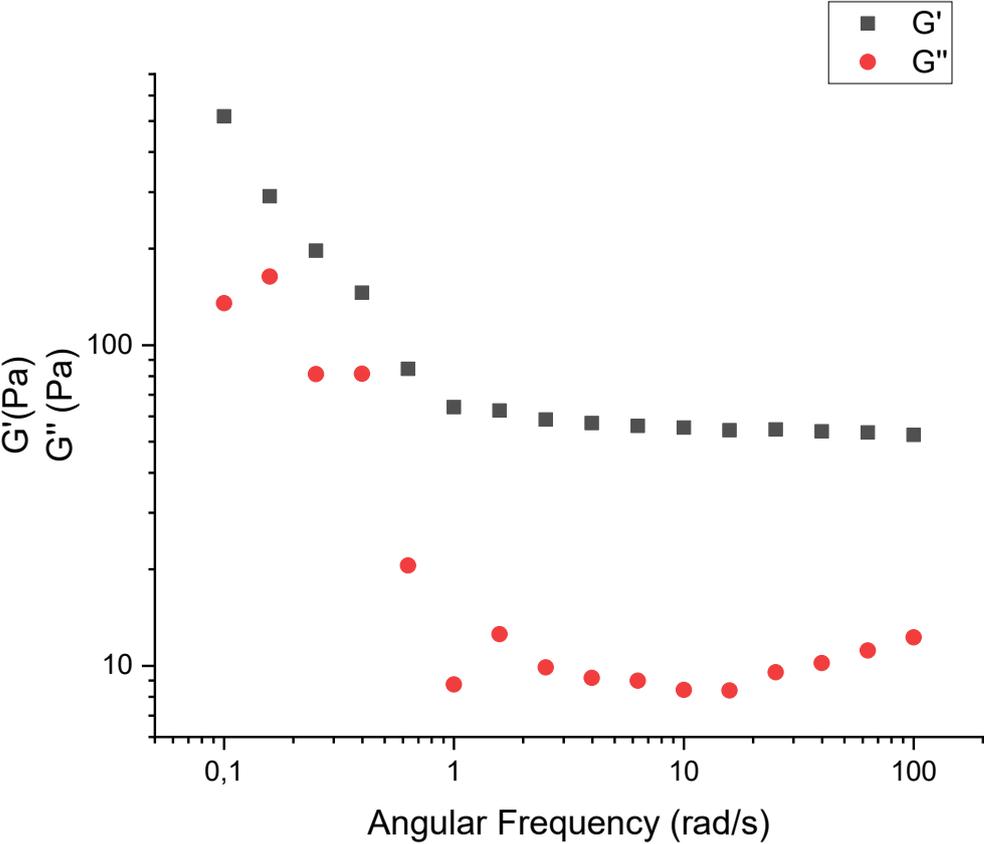
Figure 24. Storage modulus and loss modulus versus angular frequency (oscillatory shear strain = 0.1 %). Axis in logarithmic scale.

3.4 Viability assay

A qualitative viability assay was carried out to investigate if the photoinitiator concentration and the GelMA-AlgMA macromer concentrations were non-cytotoxic and allowed the embedded cells' survival. Therefore, NIH-3T3 fibroblast cells were mixed with 5 % (w/v) GelMA and 1 % (w/v) AlgMA polymer solutions with the photoinitiator LAP at 0.05 % (w/v). The initial density of the cells was $5 \cdot 10^6$ cells·mL^{-1}. The solution was loaded in the pool system previously described and exposed to UV to form disc-shaped hydrogels 250 μm in height and 6 mm in radius. The viability was evaluated using a Live/Dead cytotoxicity assay, and samples were analysed using a confocal microscope (figure 25).
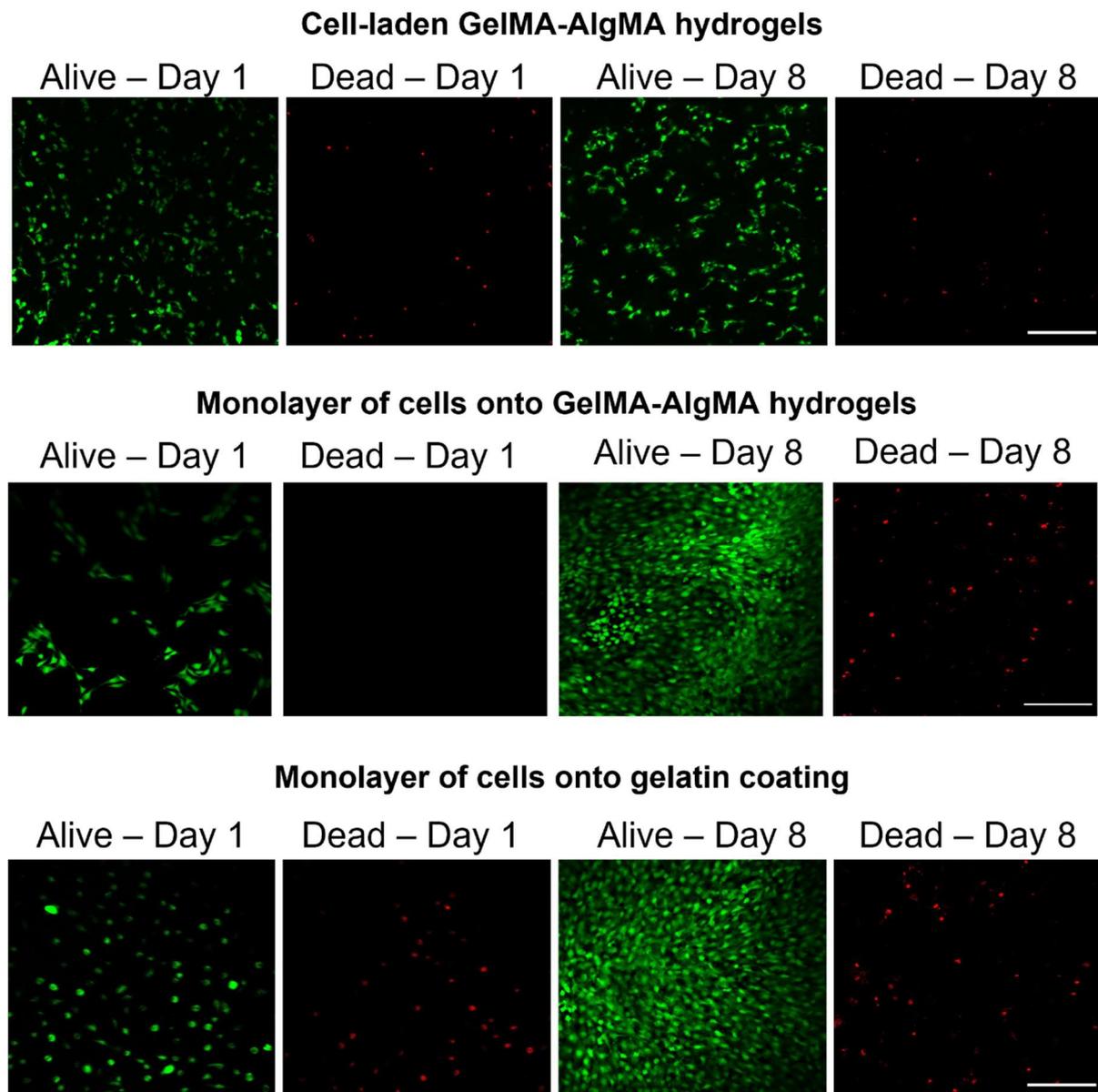
Figure 205. Live/Dead assay of fibroblasts (i) embedded in 5 % (w/v) GelMA − 1 % (w/v) AlgMA hydrogel (top, maximum intensity projection), (ii) seeded onto a 5 % (w/v) GelMA − 1 % (w/v) AlgMA hydrogel (middle) and (iii) seeded onto a gelatin-coating. Images of cells alive and dead on days 1 and 8 are shown. Scale bar: 200 μm.

Moreover, the cytotoxicity assay was also performed on the hydrogels and the gelatin coating loaded with a monolayer of cells to compare the viability of the three different constructs. In these samples, the initial density of cells was $5 \cdot 10^4$ cells·cm^{-1}. The viability for all three samples was evaluated on days 1 and 8. Figure 25 shows the confocal images of the green and red fluorescent signals for the three different samples. In particular, the images showing the cell-laden hydrogels include the whole z-stacks (100 μm) with the maximum intensity projection. It can be seen in all the pictures and regardless of the day that most NIH-3T3 cells were alive, while a minority of dead cells can be visualized.

The precise quantification of dead and live cells was performed through KNIME software [79]. The percentages of viability corresponding to each condition are expressed in figure 26. The three constructs showed excellent viability, and all the mean values were above 90 %, except for the cells onto the gelatin coating at day 1. Still, no statistical differences when compared to the other materials were observed.
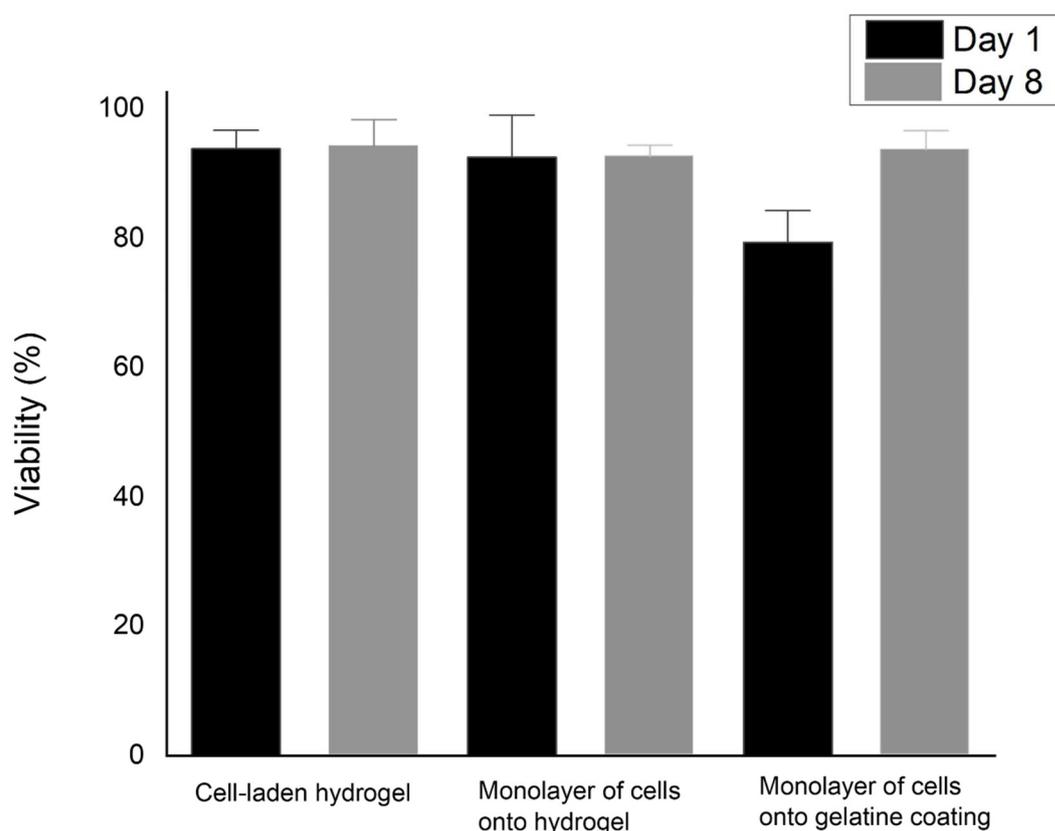
Figure 216. Viability on days 1 and 8 of NIH-3T3 cells (i) embedded in 5 % (w/v) GelMA − 1 % (w/v) AlgMA hydrogel, (ii) seeded onto a 5 % (w/v) GelMA − 1 % (w/v) AlgMA hydrogel and (iii) seeded onto a gelatin coating. Values are mean ± standard deviation, n = 9.

Figure 27 shows the 3D reconstruction of the cell-laden hydrogels on days 1 and 8, providing relevant information on cell position along with their thickness. The two images display around 100 µm of the central thickness of the hydrogel. The 3D reconstruction showing day 1 emphasizes that the hydrogel fabrication method allowed a homogenous distribution through the entire thickness after its fabrication.

3D reconstruction of cell-laden hydrogel
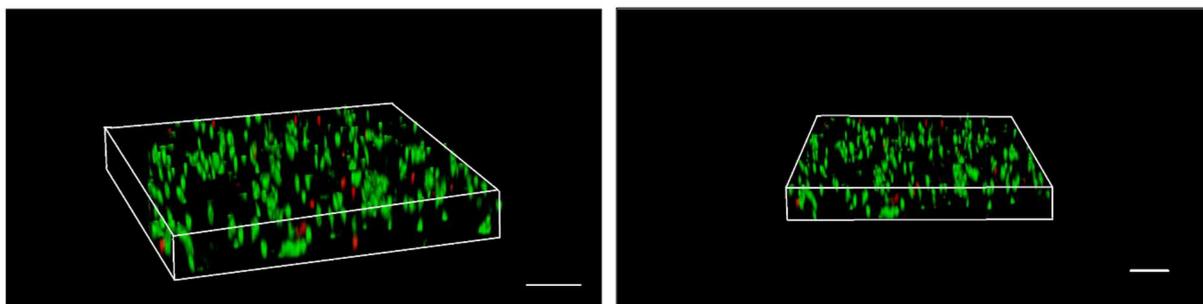
Figure 227. 3D reconstructions of fibroblasts embedded in 5 % (w/v) GelMA – 1 % (w/v) AlgMA hydrogel showing cell viability (live cells stain in green, dead cells in red) on days 1 and 8. Scale bar: 100 µm.

However, observing the entire volume (250 µm) of the hydrogel on day 8 (figure 28), it can be seen that the amount of fibroblast inside the hydrogel decreased, and the density at or near the surfaces increased. The diminished cell population inside is probably due to mass transport constraints limiting oxygen permeability and nutrient diffusion. These results are in accordance with previous findings, showing growth arrest compared to the 2D constructs with the same composition, and a decrease in cell metabolic activity was reported [80], [81], [82]. Moreover, to evaluate the growth arrest in the cell-laden hydrogels, the number of alive and dead cells on day 1 was compared to day 8 (figure 29). A statistic difference was encountered in the two-dimensional constructs, while no difference in the number of cells was observed in the cell-laden hydrogels, confirming the growth arrest.
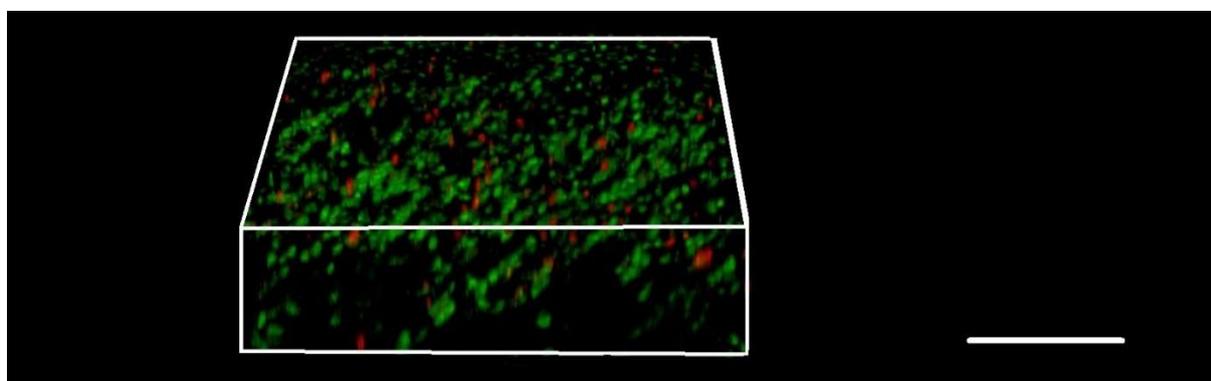
Figure 238. 3D reconstructions of fibroblasts embedded in 5 % (w/v) GelMA – 1 % (w/v) AlgMA hydrogel (entire thickness) showing cell viability (live cells stain in green, dead cells in red) on day 8. Scale bar: 250 µm.
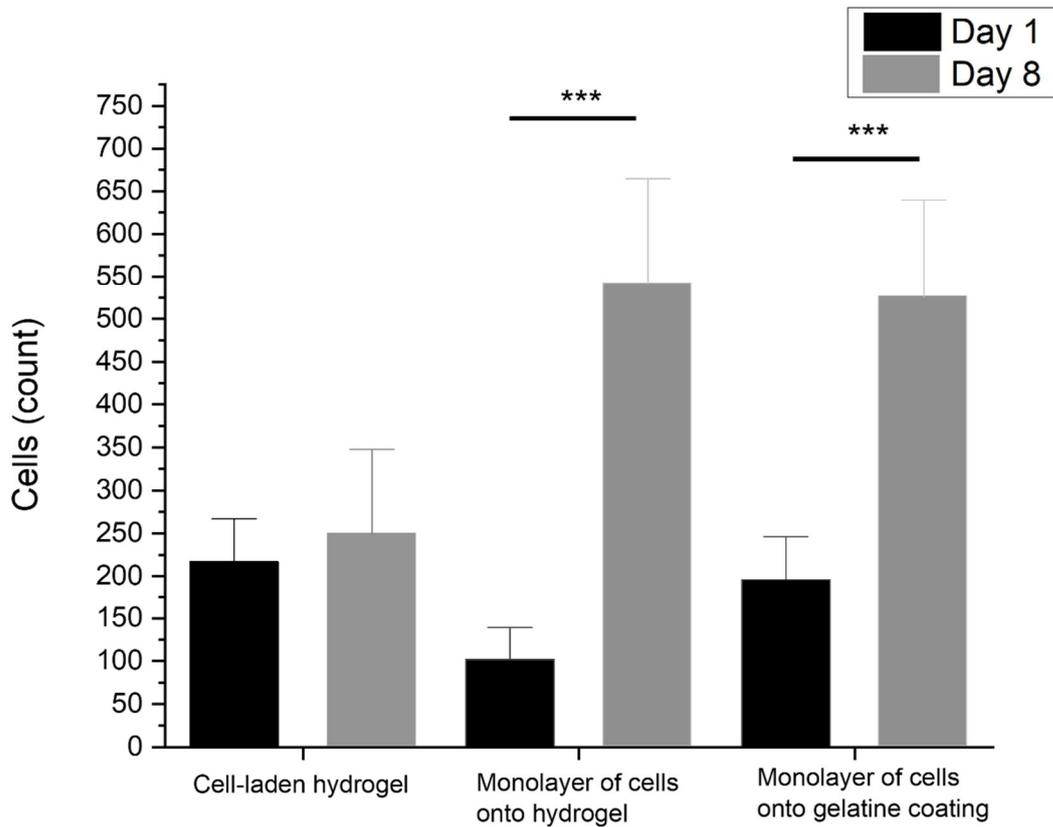
Figure 29. Number of cells on days 1 and 8 of NIH-3T3 cells (i) embedded in 5 % (w/v) GelMA − 1 % (w/v) AlgMA hydrogel, (ii) seeded onto a 5 % (w/v) GelMA − 1 % (w/v) AlgMA hydrogel and (iii) seeded onto a gelatin coating. Values are mean ± standard deviation, n = 9. ***p<0.001.

3.5 NIH-3T3 Ypet CDMs deposition

The CDMs deposition was carried out with NIH-3T3 Ypet FN cells. The CDMs production was visually monitored with an optical microscope (figure 30). Two days after seeding, the ascorbic acid treatment was started to enhance ECM production and stopped at day 10 when further analyses were performed. After day 4, the monolayers onto the hydrogel and the gelatin coating were utterly confluent. In contrast, the cells tend to reach the upper surface in the three-dimensional hydrogels and only grow in this area (the images at days 7 and 10 of cell-laden hydrogel were collected from the upper part of the hydrogel). Moreover, observing the shape of cells throughout the days in the three-dimensional environment, a round shape was encountered on the day of seeding. Nevertheless, in the following days, cells tend to elongate, achieving a three-dimensional spread morphology. Indeed, cells spread and migrate extensively in the presence of a high concentration of RGD sequences, which are present in gelatin macromer chains [83].

Cell-laden hydrogel

Day 2	Day 4	Day 7	Day 10

Monolayer of cells onto GelMA-AlgMA hydrogel

Day 2	Day 4	Day 7	Day 10

Monolayer of cells onto gelatin coating

Day 2	Day 4	Day 7	Day 10
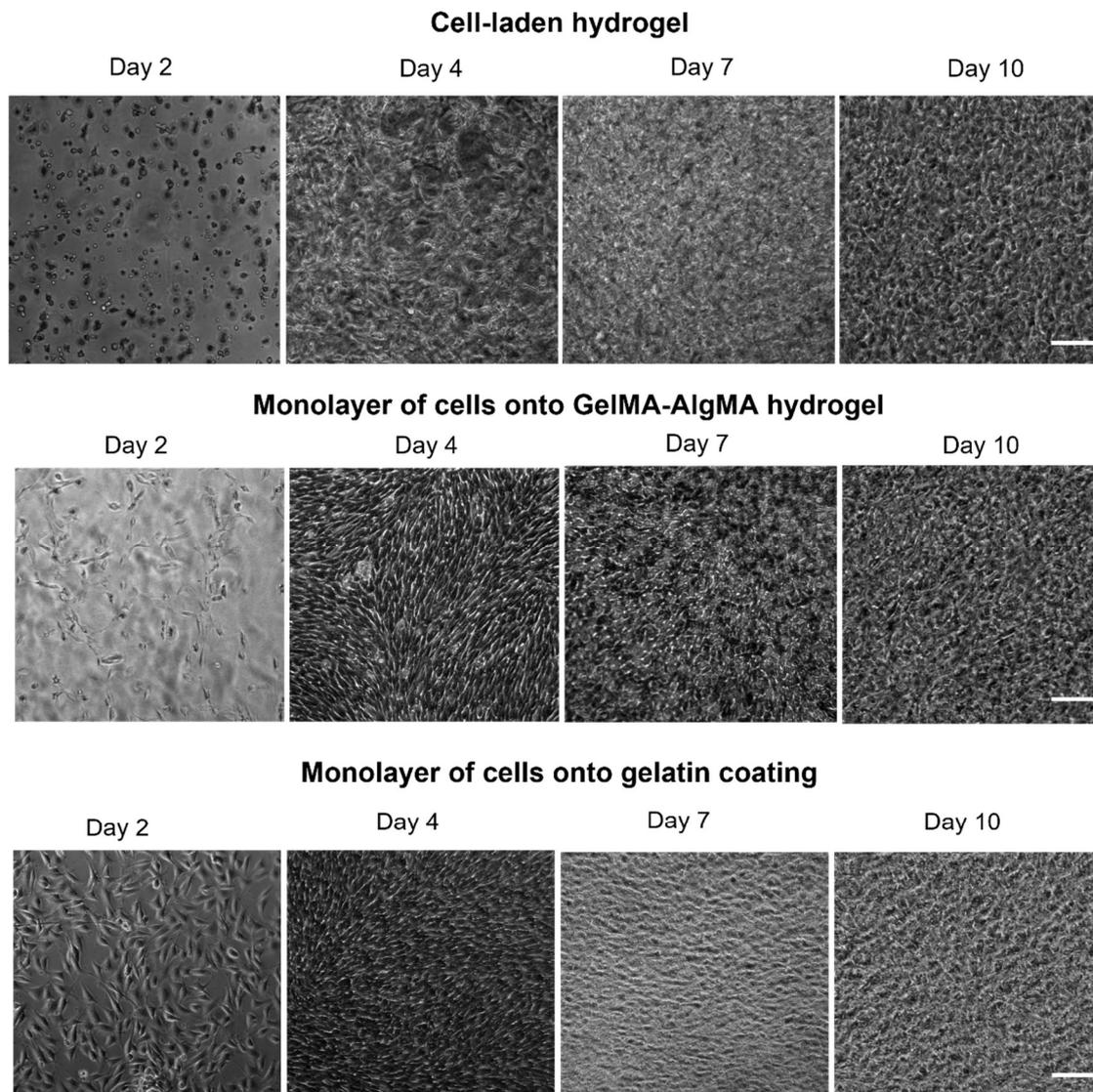
Figure 240.Fibroblasts cell-derived matrices production (i) embedded in 5 % (w/v) GelMA – 1 % (w/v) AlgMA hydrogel (top, maximum intensity projection), (ii) seeded onto a 5 % (w/v) GelMA – 1 % (w/v) AlgMA hydrogel (middle) and (iii) seeded onto a gelatin-coating. Images of cells alive and dead on days 1 and 8 are shown. Scale bar: 100 µm

Moreover, it was visually observed that the mechanical integrity of 5 % (w/v) GelMA – 1 % (w/v) AlgMA hydrogel network decreased after ten days of culture, and the loss of hydrogel shape defined contours were registered.

3.6 Cells distribution and secretion

To assess and analyse cell distribution and secretion, stainings of the three constructs were performed after ten days of culture, including eight days of ascorbic acid treatment.

Hoechst is a DNA-specific blue fluorescent dye that penetrates cells to stain nuclei of live and fixed cells [60]. Phalloidin-iFluor 594 binds with actin filaments (F-actin) and is generally used in formaldehyde-fixed tissues, cell-free experiments or cell cultures [61]. Moreover, thanks

to the genetically modified NIH-3T3 line, the fluorescently labelled fibronectin (FN) was visualized. FN is a protein secreted by cells, and it facilitates the adhesion to other ECM proteins [84]. The analysis of FN and F-actin was a preliminary test to determine if fibroblasts were proliferating and secreting ECM proteins. Recent studies have focused on the interaction between collagen VI and ECM proteins, such as FN, in collagen VI-related congenital muscular diseases (COL6-RD). Therefore, characteristics of fibronectin fibrils must be analysed to investigate the CDMs architecture of patients. Indeed, it was found that fibronectin fibrils of healthy donors were significantly thinner and less aligned than in patients' CDMs [85]. Here, it was preliminary analysed if mouse fibroblasts embedded in three-dimensional hydrogel secrete FN. Figure 31 shows fluorescent confocal microscopy pictures for the inside and the surface of the hydrogels on day 10 after encapsulation. Nuclei signal shows that cells were found in vast amounts on the surface, while inside, cells were few and didn't proliferate. F-actin signal displays that fibroblast on the surface had a well-developed actin-cytoskeleton and a spread morphology. Moreover, fibronectin was largely produced. On the contrary, fibroblasts inside the hydrogel didn't produce any fibronectin network. Nevertheless, concentrating on the F-actin signal inside the hydrogel (figure 32), it can be noticed the loss of cell round shape and the presence filopodia at their edges.

Observing the monolayers onto gelatin coating and GelMA-AlgMA hydrogel (figure 33 and 34), cells proliferate and secrete ECM proteins, agreeing with previous work [85]. The only difference encountered between the two substrates was that cells tend to remodel GelMA-AlgMA hydrogels' surface and slightly elongate inside the hydrogel.

In conclusion, the two-dimensional substrates were suitable for cells proliferation and CDMs production. Nonetheless, the three-dimensional hydrogel doesn't allow secretion of ECM proteins, resulting, for the moment, unsuitable for the purpose of analysing the collagen VI, fibronectin, and elastin fibres for COL6 RD patients' screening.
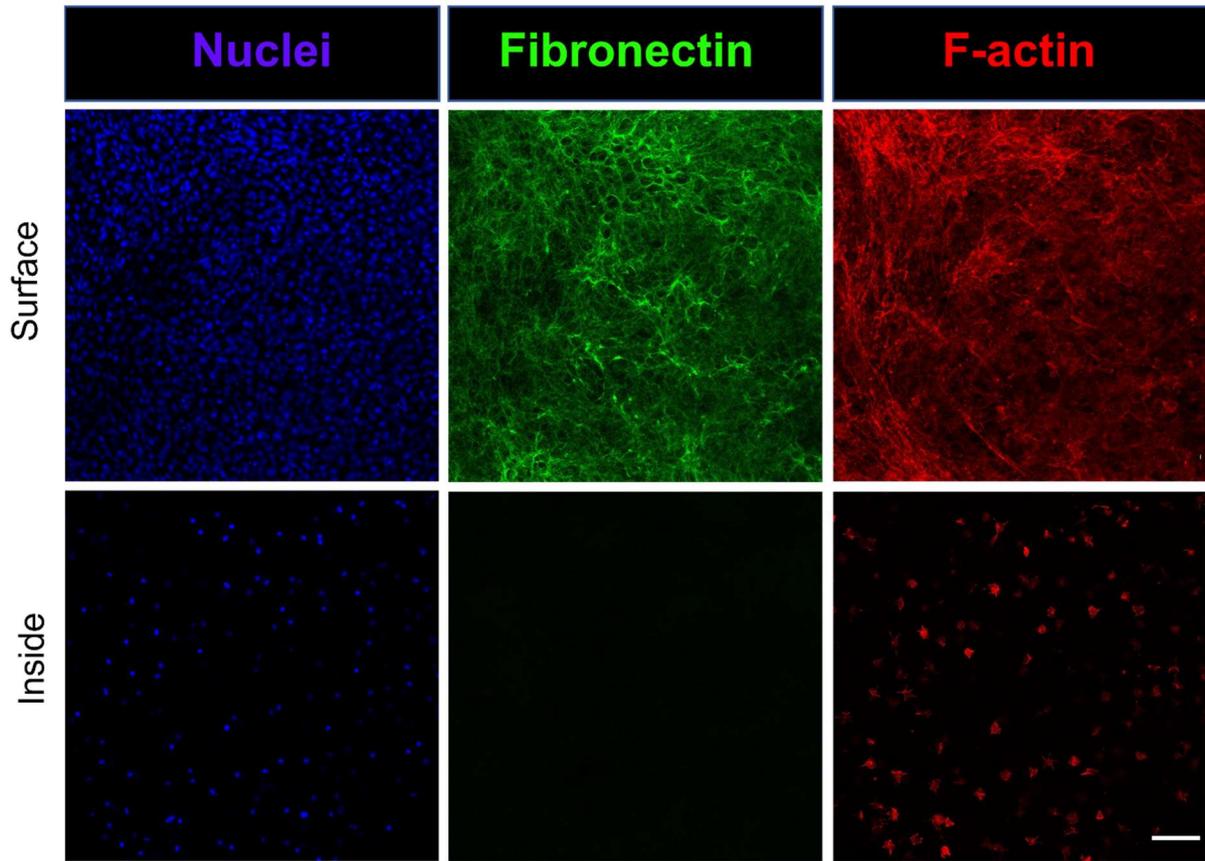
Figure 251. Staining of fibroblasts embedded in 5 % (w/v) GelMA – 1 % (w/v) AlgMA hydrogel for Nuclei and F-actin (blue and red). Fluorescent fibronectin secreted by cells is also visualized (green). Images are stacks from the surface (top panel) and from the inside (bottom panel). Scale bar: 100 µm.
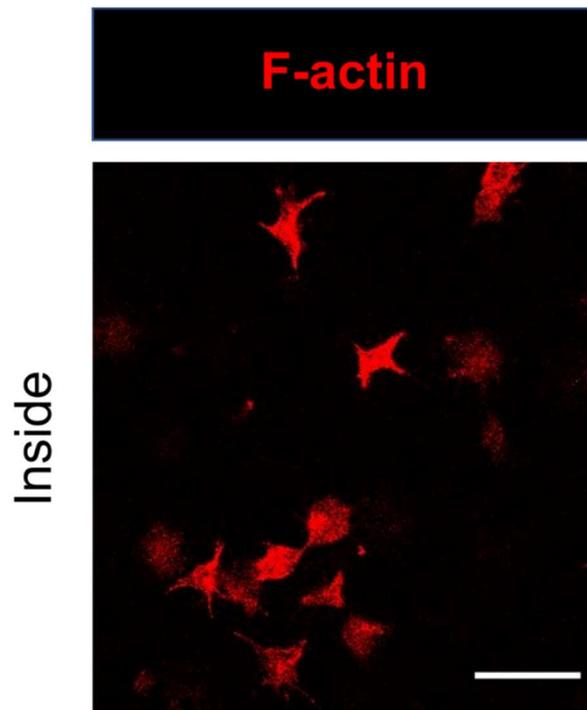
Figure 262. Zoom of the F-actin staining of fibroblasts embedded in 5 % (w/v) GelMA–1 % (w/v) AlgMA hydrogel. Scale bar 100 µm.

51

Monolayer of cells onto gelatin coating
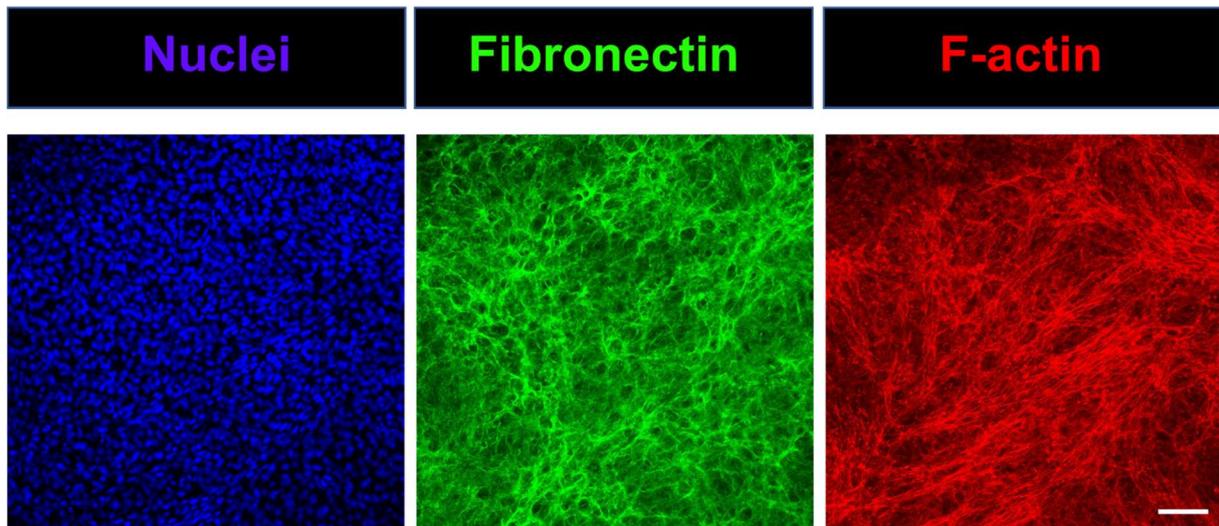
Figure 273. Staining of fibroblasts seeded onto 5 % (w/v) GelMA – 1 % (w/v) AlgMA hydrogel for Nuclei and F-actin (blue and red). Fluorescent fibronectin secreted by cells is visualized (green). Scale bar: 100 μm.

Monolayer of cells onto GelMA-AlgMA hydrogels
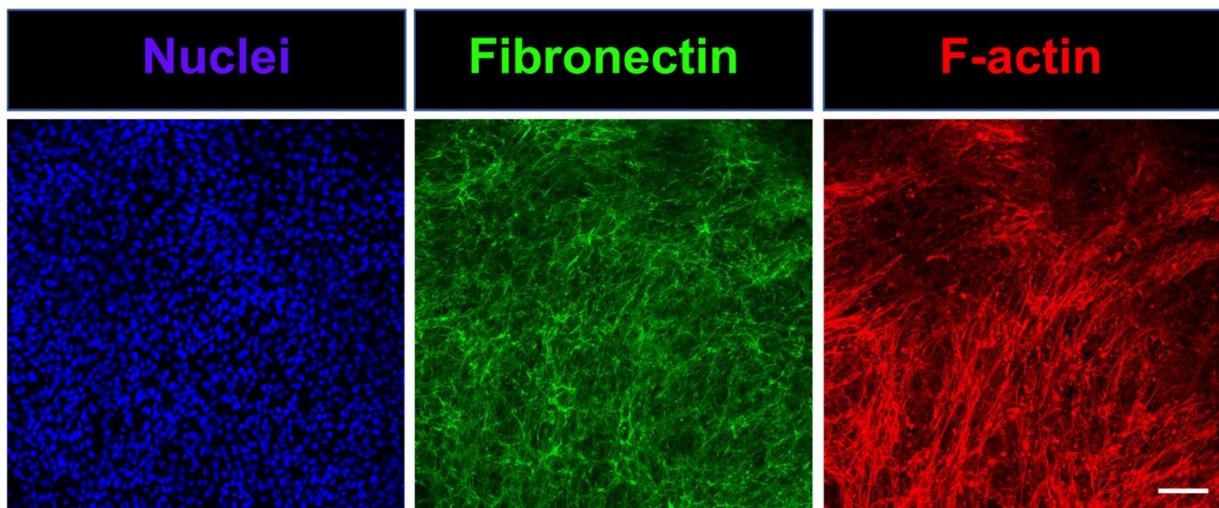
Figure 284. Staining of fibroblasts seeded onto gelatin-coating for Nuclei and F-actin (blue and red). Fluorescent fibronectin secreted by cells is visualized (green). Scale bar: 100 μm

3.7 Study about the hydrogel printability

An available strategy to overcome the lack of three-dimensionality in CDMs production could be hydrogels extrusion bioprinting. Indeed, thanks to bioprinting, different geometries can be evaluated to improve CDM deposition. Moreover, it will be possible to fabricate a 3D structure and thus seeding the cells in a 3D environment. In this regard, a study about the

ideal temperature related to viscosity and shear rate for bioprinting 5 % (w/v) GelMA and 1 % (w/v) AlgMA solution was performed.

The shear-thinning behaviour can influence the printability of the bioink. During the procedure, the bioink should exhibit low viscosity in order to avoid excessive cell shear stress and the clogging of the needle. On the contrary, the bioink should rapidly solidify after deposition to preserve shape fidelity [86].

In extrusion bioprinting, several parameters can determine the printability and the fidelity of the bioink, such as printing pressure, nozzle inner diameter, printing speed, cartridge temperature and bed temperature. Numerous studies about the ideal bioprinting parameters have been carried out for many biomaterials. Depending on the biomaterial, the printing pressure can broadly range between $5 \cdot 10^{-4}$ kPa and $4.7 \cdot 10^{5}$ kPa [87], the printing speed between 700 mm·s^{-1} and 10 μm·s^{-1} [86] (the range mainly used is 1 – 30 mm·s^{-1} [87]), the cartridge temperature vary mainly between 20 and 40 °C and bed temperature from −80 °C to 70 °C [87]. These parameters influence bioink viscosities that can extend between 30 to $6 \cdot 10^{7}$ mPa·s [86], [88]. However, He *et al*. have found that the optimum range for a mixture of gelatin and alginate was between 300 and $3 \cdot 10^{4}$ mPa·s [89].

To analyse the ability of the ink to flow under external forces, a rheology study should be performed. Shear rate sweeps test is employed to predict how the bioink behaves during the process. In particular, viscosity is determined depending on the shear rate. This test was performed at different temperatures to assess which temperature would be the most suitable for bioprinting. Figure 35 shows the viscosity at 5, 10, 15, 20, 25 °C. It can be seen that at 25 °C the viscosity is very low and thus not suitable for bioprinting. Therefore, temperatures between 20° C and 25°C were further analysed (figure 36). The bioink should have a low viscosity during the printing process to preserve cells viability but high viscosity would be ideal for maintaining the fabricated structure after the extrusion when almost no shear forces are exerted on the solution. According to the optimum range found by He *et al.,* the ideal printing temperature would be 21 °C. At this temperature, the solution presents the viscosity around 10^{3} mPa·s for a shear rate of 100 s^{-1} and around 10^{4} mPa·s for a shear rate of 1 s^{-1}.
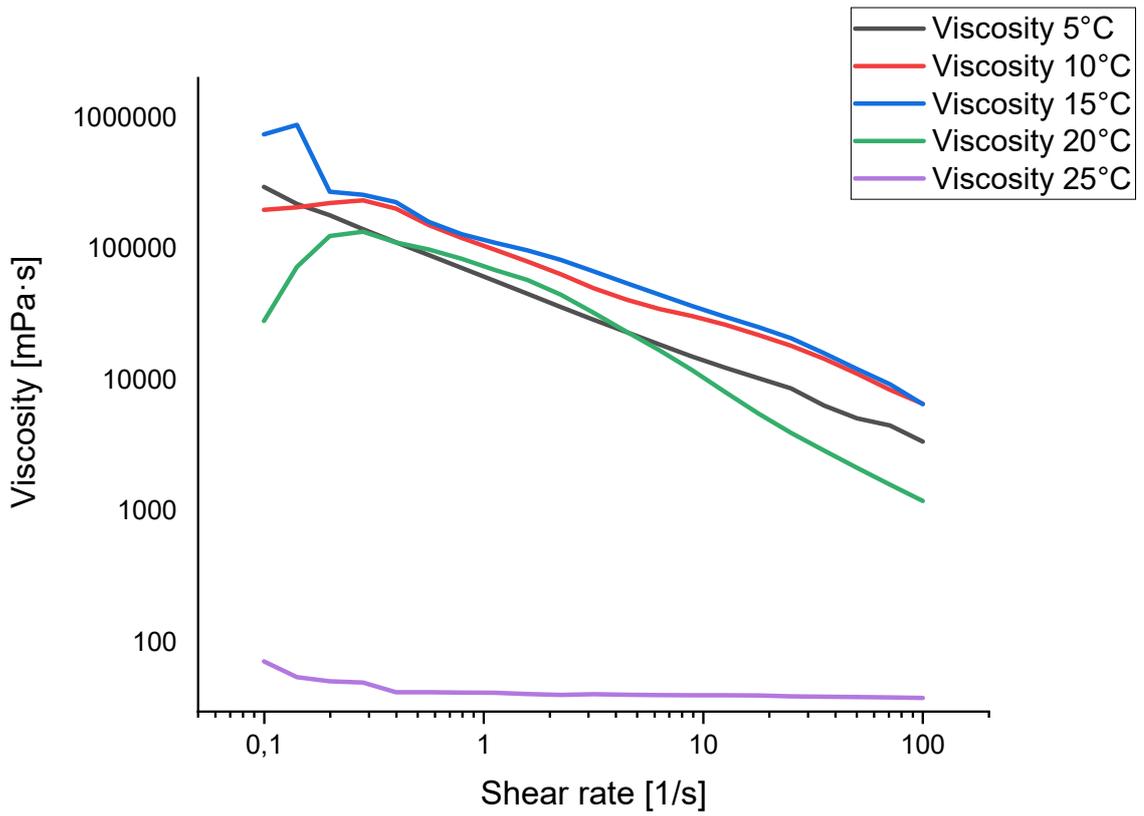
Figure 29. Viscosity versus shear rate for the 5 % (w/v) – 1% hydrogel at different temperatures. Axis in logarithmic scale.
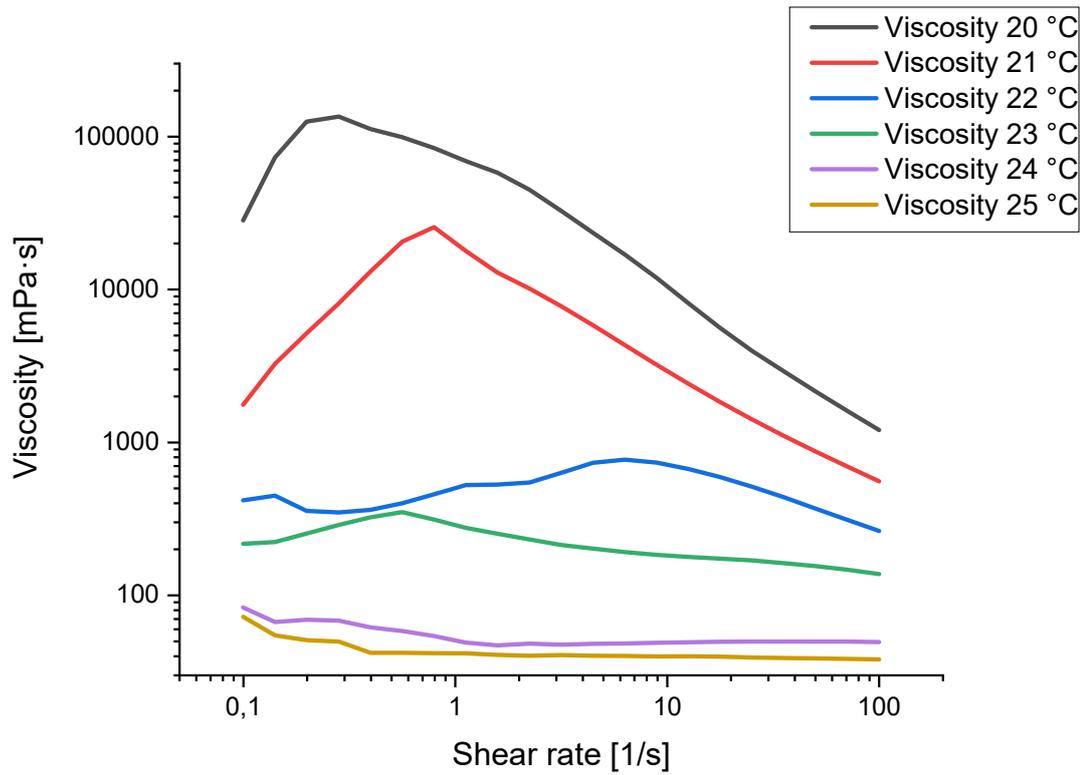
Figure 30. Viscosity versus shear rate for the 5 % (w/v) – 1% hydrogel at different temperatures. Axis in logarithmic

4 Discussion and future development

The two most affected tissues in COL6-RD are muscle and skin. They are abundant in fibroblasts, which are the main sources of collagen VI, resulting in the cell type that mainly impacts these diseases [90]. Therefore, one of the first screening carried out for the disease diagnosis is to evaluate collagen VI secretions in *in vitro* patients' fibroblasts culture [91]. Furthermore, patients present not only alterations in collagen VI but also in its integration with other extracellular matrices (ECM) fundamental components, such as elastin, fibronectin, fibrillin I, which can be analysed to perform patients' screening. Hence, skin fibroblasts can be employed to fabricate *in vitro* cell-derived matrices (CDMs) to reproduce the biological variability of COL6-RD and the key pathological features.

2D constructs for CDM production have been recently developed and have shown excellent results for disease screening. In particular, skin fibroblasts from patients with a severe and mild form of the disease were seeded onto a gelatin coating to produce CDMs. Moreover, the developed models were promising for exploring the alterations of the matrix organization. However, 2D models fail to replicate the heterogeneous three-dimensional structure of tissues. Therefore, a comparison between two bi-dimensional models and one three-dimensional was carried out in this work.

The primary step for developing CDM models is the choice of the biomaterial for cell culture. Indeed, its water content, mechanical properties, porous dimension, cell remodelling capabilities should be the most similar to the *in vivo* ECM. Furthermore, the material should be non-toxic and biodegradable, ideally matching the degradation time with the new ECM production time, avoiding issues of mechanical integrity.

To fit these requirements, GelMA – AlgMA hydrogel co-network was chosen. GelMA is a natural polymer derived from gelatin, but gelatin can not be UV photocrosslinked. It was decided to employ gelatin methacryloyl because pure gelatin is not stable at 37 °C. GelMA preserves many gelatin properties, like cell adhesion motifs and highly biodegradability [32]. However, one of the problems when using natural hydrogels for long-term cell culture is the fast hydrogel degradation that limits the mechanical stability of the constructs during ECM deposition. Therefore, to minimize biodegradability and produce a long-lasting hydrogel, AlgMA was added to the network. AlgMA is a biocompatible and non-toxic biomaterial, able to increase the degradation rate and the swelling properties of bare GelMA. ECM has a

water content of about 75 %, and therefore hydrogel ability to store a high quantity of water is crucial for mimicking the physiological environment [92].

After the production of the polymers, the methacrylation was verified through H-NMR, and the degree of functionalization was calculated. The degree of functionalization is relevant because it indicates how densely packed is the internal network, strongly influencing cell survival and secretion. Moreover, the biomaterial properties were analysed, such as degradation rate, swelling ratio, compressive modulus, and rheological behaviour. The obtained results were compared with the literature showing that the hydrogel had suitable properties for cell culture.

Hence, mouse fibroblasts were cultured both embedded in the gel and as a monolayer on the top of the hydrogel and compared to the conventional gelatine coating. First of all, it was corroborated that neither the materials employed nor the UV photopolymerization to fabricate the hydrogels was toxic for cells. It is well-documented that UV light can induce the phosphorylation of the DNA, producing DNA alteration. However, the high viability encountered may suggest that this did not occur in the model thanks to the low photoinitiator concentration and UV energy dose [93].

However, the results of the cell-laden hydrogel show that cells were alive but in growth arrest. Therefore, they didn't proliferate and secrete ECM proteins due to low macronutrient diffusion and cell stress problems. On the contrary, 2D models showed high ECM production, and therefore, they remain the most suitable choice for CDM production for COL6-RD patient screening. However, new strategies should be developed to effectively produce 3D models for CDM production. In this regard, extrusion bioprinting may pave the way for further study about 3D CDM models based on GelMA - AlgMA hydrogel.

At this stage of knowledge, CDM produced in a two-dimensional environment can be employed to reproduce differences in ECM architecture and composition *in vitro*. Overall, CDM constructs present a native-like composition that cannot be reached with other *in vitro* technologies. Therefore, it will be of major importance to develop 3D CDM models to resume both native-like composition and 3D environment, addressing the need for specific models for COL6-RD patients.

5 Bibliography

[1]   C. Jimenez-Mallebrera, S. C. Brown, C. A. Sewry, and F. Muntoni, "Congenital muscular dystrophy: Molecular and cellular aspects," *Cell. Mol. Life Sci.*, vol. 62, no. 7–8, pp. 809–823, 2005, doi: 10.1007/s00018-004-4510-4.

[2]   A. Graziano *et al.*, "Prevalence of congenital muscular dystrophy in Italy: A population study," *Neurology*, vol. 84, no. 9, pp. 904–911, 2015, doi: 10.1212/WNL.0000000000001303.

[3]   M. Cescon, F. Gattazzo, P. Chen, and P. Bonaldo, "Collagen VI at a glance," *J. Cell Sci.*, vol. 128, no. 19, pp. 3525–3531, 2015, doi: 10.1242/jcs.169748.

[4]   M. Antoniel *et al.*, "Tendon Extracellular Matrix Remodeling and Defective Cell Polarization in the Presence of Collagen VI Mutations," *Cells*, vol. 9, no. 2, 2020, doi: 10.3390/cells9020409.

[5]   S. Paco *et al.*, "Gene Expression Profiling Identifies Molecular Pathways Associated with Collagen VI Deficiency and Provides Novel Therapeutic Targets," *PLoS One*, vol. 8, no. 10, pp. 1–15, 2013, doi: 10.1371/journal.pone.0077430.

[6]   R. J. Butterfield *et al.*, "Position of glycine substitutions in the triple helix of COL6A1, COL6A2, and COL6A3 is correlated with severity and mode of inheritance in collagen vi myopathies," *Hum. Mutat.*, vol. 34, no. 11, pp. 1558–1567, 2013, doi: 10.1002/humu.22429.

[7]   H. Xing, H. Lee, L. Luo, and T. R. Kyriakides, "Extracellular matrix-derived biomaterials in engineering cell function," *Biotechnol. Adv.*, vol. 42, no. October 2018, p. 107421, 2020, doi: 10.1016/j.biotechadv.2019.107421.

[8]   G. Rubi-Sans, O. Castaño, I. Cano, M. A. Mateos-Timoneda, S. Perez-Amodio, and E. Engel, "Engineering Cell-Derived Matrices: From 3D Models to Advanced Personalized Therapies," *Adv. Funct. Mater.*, vol. 30, no. 44, pp. 1–19, 2020, doi: 10.1002/adfm.202000496.

[9]   A. V. Giraut, "Tesi doctoral," *Anu. la Soc. Catalana Filos.*, vol. 0, no. 17, pp. 273-280–

280, 2006, doi: 10.2436/ascf.v0i17.2103.

[10]   R. Kaukonen, G. Jacquemet, H. Hamidi, and J. Ivaska, "Cell-derived matrices for studying cell proliferation and directional migration in a complex 3D microenvironment," *Nat. Protoc.*, vol. 12, no. 11, pp. 2376–2390, 2017, doi: 10.1038/nprot.2017.107.

[11]   T. Hoshiba and J. Gong, "Fabrication of cell-derived decellularized matrices on three-dimensional (3D)-printed biodegradable polymer scaffolds," *Microsyst. Technol.*, vol. 24, no. 1, pp. 613–617, 2018, doi: 10.1007/s00542-017-3470-1.

[12]   J. Franco-Barraza, D. A. Beacham, M. D. Amatangelo, and E. Cukierman, "Preparation of extracellular matrices produced by cultured and primary fibroblasts," *Curr. Protoc. Cell Biol.*, vol. 2016, pp. 10.9.1-10.9.34., 2016, doi: 10.1002/cpcb.2.

[13]   H. Lu, T. Hoshiba, N. Kawazoe, I. Koda, M. Song, and G. Chen, "Cultured cell-derived extracellular matrix scaffolds for tissue engineering," *Biomaterials*, vol. 32, no. 36, pp. 9658–9666, 2011, doi: 10.1016/j.biomaterials.2011.08.091.

[14]   D. Park *et al.*, "Extracellular matrix anisotropy is determined by TFAP2C-dependent regulation of cell collisions," *Nat. Mater.*, vol. 19, no. 2, pp. 227–238, 2020, doi: 10.1038/s41563-019-0504-3.

[15]   E. Almici, D. Caballero, J. Montero, and J. Samitier, *3D neuroblastoma in vitro models using engineered cell-derived matrices*. INC, 2020.

[16]   R. Castelló-Cros and E. Cukierman, "Stromagenesis during tumorigenesis: characterization of tumor-associated fibroblasts and stroma-derived 3D matrices.," *Methods Mol. Biol.*, vol. 522, pp. 275–305, 2009, doi: 10.1007/978-1-59745-413-1_19.

[17]   K. Matsuura, R. Utoh, K. Nagase, and T. Okano, "Cell sheet approach for tissue engineering and regenerative medicine," *J. Control. Release*, vol. 190, pp. 228–239, 2014, doi: 10.1016/j.jconrel.2014.05.024.

[18]   G. Tour, M. Wendel, and I. Tcacencu, "Cell-derived matrix enhances osteogenic properties of hydroxyapatite," *Tissue Eng. - Part A*, vol. 17, no. 1–2, pp. 127–137, 2011, doi: 10.1089/ten.tea.2010.0175.

[19]   X. Zhou, A. Yang, Z. Huang, G. Yin, X. Pu, and J. Jin, "Enhancement of neurite adhesion,

alignment and elongation on conductive polypyrrole-poly(lactide acid) fibers with cell-derived extracellular matrix," *Colloids Surfaces B Biointerfaces*, vol. 149, pp. 217–225, 2017, doi: 10.1016/j.colsurfb.2016.10.014.

[20]   H. Geckil, F. Xu, X. Zhang, S. Moon, and U. Demirci, "Engineering hydrogels as extracellular matrix mimics," *Nanomedicine*, vol. 5, no. 3, pp. 469–484, 2010, doi: 10.2217/nnm.10.12.

[21]   N. A. Peppas, P. Bures, W. Leobandung, and H. Ichikawa, "Hydrogels in pharmaceutical formulations," *Eur. J. Pharm. Biopharm.*, vol. 50, no. 1, pp. 27–46, 2000, doi: 10.1016/S0939-6411(00)00090-4.

[22]   S. Van Vlierberghe, P. Dubruel, and E. Schacht, "Biopolymer-based hydrogels as scaffolds for tissue engineering applications: A review," *Biomacromolecules*, vol. 12, no. 5, pp. 1387–1408, 2011, doi: 10.1021/bm200083n.

[23]   E. González-Díaz and S. Varghese, "Hydrogels as Extracellular Matrix Analogs," *Gels*, vol. 2, no. 3, p. 20, 2016, doi: 10.3390/gels2030020.

[24]   J. L. Ifkovits, J. A. Burdick, and D. Ph, "Review : Photopolymerizable and Degradable," vol. 13, no. 10, 2007, doi: 10.1089/ten.2007.0093.

[25]   F. Ullah, M. B. H. Othman, F. Javed, Z. Ahmad, and H. M. Akil, "Classification, processing and application of hydrogels: A review," *Mater. Sci. Eng. C*, vol. 57, pp. 414–433, 2015, doi: 10.1016/j.msec.2015.07.053.

[26]   M. W. Tibbitt and K. S. Anseth, "Hydrogels as extracellular matrix mimics for 3D cell culture," *Biotechnol. Bioeng.*, vol. 103, no. 4, pp. 655–663, 2009, doi: 10.1002/bit.22361.

[27]   A. Bossion *et al.*, "Opportunities for organocatalysis in polymer synthesis via step-growth methods," *Prog. Polym. Sci.*, vol. 90, pp. 164–210, 2019, doi: 10.1016/j.progpolymsci.2018.11.003.

[28]   T. Greene, T. Y. Lin, O. M. Andrisani, and C. C. Lin, "Comparative study of visible light polymerized gelatin hydrogels for 3D culture of hepatic progenitor cells," *J. Appl. Polym. Sci.*, vol. 134, no. 11, pp. 1–10, 2017, doi: 10.1002/app.44585.

[29]   D. Zhou and Y. Ito, "Visible light-curable polymers for biomedical applications," *Sci.*

China Chem., vol. 57, no. 4, pp. 510–521, 2014, doi: 10.1007/s11426-014-5069-z.

[30] H. Shih and C. C. Lin, "Visible-light-mediated thiol-ene hydrogelation using eosin-Y as the only photoinitiator," *Macromol. Rapid Commun.*, vol. 34, no. 3, pp. 269–273, 2013, doi: 10.1002/marc.201200605.

[31] A. I. Van Den Bulcke, B. Bogdanov, N. De Rooze, E. H. Schacht, M. Cornelissen, and H. Berghmans, *Biomacromolecules*, vol. 1, no. 1, pp. 31–38, 2000.

[32] S. Xiao *et al.*, "Gelatin Methacrylate (GelMA)-Based Hydrogels for Cell Transplantation: an Effective Strategy for Tissue Engineering," *Stem Cell Rev. Reports*, vol. 15, no. 5, pp. 664–679, 2019, doi: 10.1007/s12015-019-09893-4.

[33] M. Sun, X. Sun, Z. Wang, S. Guo, G. Yu, and H. Yang, "Synthesis and properties of gelatin methacryloyl (GelMA) hydrogels and their recent applications in load-bearing tissue," *Polymers (Basel).*, vol. 10, no. 11, 2018, doi: 10.3390/POLYM10111290.

[34] W. Schuurman *et al.*, "Gelatin-methacrylamide hydrogels as potential biomaterials for fabrication of tissue-engineered cartilage constructs," *Macromol. Biosci.*, vol. 13, no. 5, pp. 551–561, 2013, doi: 10.1002/mabi.201200471.

[35] P. Xu *et al.*, "Stiffness of photocrosslinkable gelatin hydrogel influences nucleus pulposus cell propertiesin vitro," *J. Cell. Mol. Med.*, vol. 25, no. 2, pp. 880–891, 2021, doi: 10.1111/jcmm.16141.

[36] L. E. Bertassoni *et al.*, "Direct-write bioprinting of cell-laden methacrylated gelatin hydrogels," *Biofabrication*, vol. 6, no. 2, 2014, doi: 10.1088/1758-5082/6/2/024105.

[37] O. Zedadra *et al.*, "Title," *Sustain.*, vol. 11, no. 1, pp. 1–14, 2019,

[38] A. García-Lizarribar, X. Fernández-Garibay, F. Velasco-Mallorquí, A. G. Castaño, J. Samitier, and J. Ramon-Azcon, "Composite Biomaterials as Long-Lasting Scaffolds for 3D Bioprinting of Highly Aligned Muscle Tissue," *Macromol. Biosci.*, vol. 18, no. 10, pp. 1–13, 2018, doi: 10.1002/mabi.201800167.

[39] J. W. Nichol, S. T. Koshy, H. Bae, C. M. Hwang, S. Yamanlar, and A. Khademhosseini, "Cell-laden microengineered gelatin methacrylate hydrogels," *Biomaterials*, vol. 31, no. 21, pp. 5536–5544, 2010, doi: 10.1016/j.biomaterials.2010.03.064.

[40]   I. Pepelanova, K. Kruppa, T. Scheper, and A. Lavrentieva, "Gelatin-methacryloyl (GelMA) hydrogels with defined degree of functionalization as a versatile toolkit for 3D cell culture and extrusion bioprinting," *Bioengineering*, vol. 5, no. 3, 2018, doi: 10.3390/bioengineering5030055.

[41]   L. Fan *et al.*, "Directing Induced Pluripotent Stem Cell Derived Neural Stem Cell Fate with a Three-Dimensional Biomimetic Hydrogel for Spinal Cord Injury Repair," *ACS Appl. Mater. Interfaces*, vol. 10, no. 21, pp. 17742–17755, 2018, doi: 10.1021/acsami.8b05293.

[42]   F. Behavior, "E ff ects of Gelatin Methacrylate Bio-ink Concentration on Mechano-Physical Properties and Human Dermal."

[43]   K. Yong and D. J. Mooney, "Progress in Polymer Science Alginate : Properties and biomedical applications," *Prog. Polym. Sci.*, vol. 37, no. 1, pp. 106–126, 2012, doi: 10.1016/j.progpolymsci.2011.06.003.

[44]   M. Tavafoghi *et al.*, "Engineering Tough, Injectable, Naturally Derived, Bioadhesive Composite Hydrogels," *Adv. Healthc. Mater.*, vol. 9, no. 10, pp. 1–12, 2020, doi: 10.1002/adhm.201901722.

[45]   F. Paquin, J. Rivnay, A. Salleo, N. Stingelin, and C. Silva, "Multi-phase semicrystalline microstructures drive exciton dissociation in neat plastic semiconductors," *J. Mater. Chem. C*, vol. 3, pp. 10715–10722, 2015, doi: 10.1039/b000000x.

[46]   S. Vijayavenkataraman, W. C. Yan, W. F. Lu, C. H. Wang, and J. Y. H. Fuh, "3D bioprinting of tissues and organs for regenerative medicine," *Adv. Drug Deliv. Rev.*, vol. 132, pp. 296–332, 2018, doi: 10.1016/j.addr.2018.07.004.

[47]   S. V. Murphy and A. Atala, "3D bioprinting of tissues and organs," *Nat. Biotechnol.*, vol. 32, no. 8, pp. 773–785, 2014, doi: 10.1038/nbt.2958.

[48]   E. S. Bishop *et al.*, "3-D bioprinting technologies in tissue engineering and regenerative medicine: Current and future trends," *Genes Dis.*, vol. 4, no. 4, pp. 185–195, 2017, doi: 10.1016/j.gendis.2017.10.002.

[49]   V. Tran and X. Wen, *Rapid prototyping technologies for tissue regeneration*. Woodhead Publishing Limited, 2014.

[50] B. Guillotin *et al.*, "Laser assisted bioprinting of engineered tissue with high cell density and microscale organization," *Biomaterials*, vol. 31, no. 28, pp. 7250–7256, 2010, doi: 10.1016/j.biomaterials.2010.05.055.

[51] K. Yue, G. Trujillo-de Santiago, M. M. Alvarez, A. Tamayol, N. Annabi, and A. Khademhosseini, "Synthesis, properties, and biomedical applications of gelatin methacryloyl (GelMA) hydrogels," *Biomaterials*, vol. 73, pp. 254–271, 2015, doi: 10.1016/j.biomaterials.2015.08.045.

[52] D. Liu, M. Nikoo, P. Zhou, and J. M. Regenstein, "Collagen and Gelatin," pp. 527–559, doi: 10.1146/annurev-food-031414-111800.

[53] H. Li, C. Tan, and L. Li, "Review of 3D printable hydrogels and constructs," *Mater. Des.*, vol. 159, pp. 20–38, 2018, doi: 10.1016/j.matdes.2018.08.023.

[54] O. Jeon, K. H. Bouhadir, J. M. Mansour, and E. Alsberg, "Photocrosslinked alginate hydrogels with tunable biodegradation rates and mechanical properties," *Biomaterials*, vol. 30, no. 14, pp. 2724–2734, 2009, doi: 10.1016/j.biomaterials.2009.01.034.

[55] C. Claaßen *et al.*, "Quantification of Substitution of Gelatin Methacryloyl: Best Practice and Current Pitfalls," *Biomacromolecules*, vol. 19, no. 1, pp. 42–52, 2018, doi: 10.1021/acs.biomac.7b01221.

[56] F. Araiza-verduzco, E. Rodr, H. Cruz, and M. Alatorre-meda, "with Modulable Mechanical Properties : E ff ect of the Molecular Conformation and Electron Density of the Methacrylate Reactive Group."

[57] A. Mignon *et al.*, "Combinatory approach of methacrylated alginate and acid monomers for concrete applications," *Carbohydr. Polym.*, vol. 155, pp. 448–455, 2017, doi: 10.1016/j.carbpol.2016.08.102.

[58] T. Mezger, *The Rheology Handbook*. 2020.

[59] A. L. Godeau, H. Delanoë-Ayari, and D. Riveline, "Generation of fluorescent cell-derived-matrix to study 3D cell migration," *Methods Cell Biol.*, vol. 156, pp. 185–203, 2020, doi: 10.1016/bs.mcb.2019.11.013.

[60] I. P. Information, "Hoechst 33342," *Cold Spring Harb. Protoc.*, vol. 2006, no. 1, p.

pdb.caut447, 2006, doi: 10.1101/pdb.caut447.

[61] P. Mhz and R. F. Powerharvester, "Product Datasheet Product Datasheet," pp. 1–12, 2015.

[62] Invitrogen Molecular Probes, "LIVE/DEAD Viability/Cytotoxicity Kit for mammalian cells," *Prod. Information, Cat. number MP 03224*, pp. 1–7, 2005, [Online]. Available: https://tools.lifetechnologies.com/content/sfs/manuals/mp03224.pdf.

[63] J. C. Yen, F. J. Chang, and S. Chang, "A New Criterion for Automatic Multilevel Thresholding," *IEEE Trans. Image Process.*, vol. 4, no. 3, pp. 370–378, 1995, doi: 10.1109/83.366472.

[64] S. Chen, "Chaotic spread spectrum watermarking for remote sensing images," *J. Electron. Imaging*, vol. 13, no. 1, p. 220, 2004, doi: 10.1117/1.1631316.

[65] X. Li *et al.*, "3D culture of chondrocytes in gelatin hydrogels with different stiffness," *Polymers (Basel).*, vol. 8, no. 8, 2016, doi: 10.3390/polym8080269.

[66] D. Loessner *et al.*, "Functionalization, preparation and use of cell-laden gelatin methacryloyl-based hydrogels as modular tissue culture platforms," *Nat. Protoc.*, vol. 11, no. 4, pp. 727–746, 2016, doi: 10.1038/nprot.2016.037.

[67] M. Zhu, Y. Wang, G. Ferracci, J. Zheng, N. J. Cho, and B. H. Lee, "Gelatin methacryloyl and its hydrogels with an exceptional degree of controllability and batch-to-batch consistency," *Sci. Rep.*, vol. 9, no. 1, pp. 1–13, 2019, doi: 10.1038/s41598-019-42186-x.

[68] Gibco Life Technologies, "Product Information Collagenase," no. X, pp. 1–2, 2013, [Online]. Available: www.lifetechnologies.com.

[69] S. Pedron and B. A. C. Harley, "Impact of the biophysical features of a 3D gelatin microenvironment on glioblastoma malignancy," *J. Biomed. Mater. Res. - Part A*, vol. 101, no. 12, pp. 3404–3415, 2013, doi: 10.1002/jbm.a.34637.

[70] A. Jabłońska-Trypuć, M. Matejczyk, and S. Rosochacki, "Matrix metalloproteinases (MMPs), the main extracellular matrix (ECM) enzymes in collagen degradation, as a target for anticancer drugs," *J. Enzyme Inhib. Med. Chem.*, vol. 31, no. March, pp. 177–183, 2016, doi: 10.3109/14756366.2016.1161620.

[71] M. Tavafoghi *et al.*, "Engineering Tough, Injectable, Naturally Derived, Bioadhesive Composite Hydrogels," *Adv. Healthc. Mater.*, vol. 9, no. 10, 2020, doi: 10.1002/adhm.201901722.

[72] B. D. Fairbanks, M. P. Schwartz, C. N. Bowman, and K. S. Anseth, "Photoinitiated polymerization of PEG-diacrylate with lithium phenyl-2,4,6-trimethylbenzoylphosphinate: polymerization rate and cytocompatibility," *Biomaterials*, vol. 30, no. 35, pp. 6702–6707, 2009, doi: 10.1016/j.biomaterials.2009.08.055.

[73] E. Monferrer *et al.*, "A three-dimensional bioprinted model to evaluate the effect of stiffness on neuroblastoma cell cluster dynamics and behavior," *Sci. Rep.*, vol. 10, no. 1, pp. 1–12, 2020, doi: 10.1038/s41598-020-62986-w.

[74] D. R. Picout and S. B. Ross-Murphy, "Rheology of biopolymer solutions and gels.," *ScientificWorldJournal.*, vol. 3, pp. 105–121, 2003, doi: 10.1100/tsw.2003.15.

[75] J. Yin, M. Yan, Y. Wang, J. Fu, and H. Suo, "3D Bioprinting of Low-Concentration Cell-Laden Gelatin Methacrylate (GelMA) Bioinks with a Two-Step Cross-linking Strategy," *ACS Appl. Mater. Interfaces*, vol. 10, no. 8, pp. 6849–6857, 2018, doi: 10.1021/acsami.7b16059.

[76] M. Bartnikowski, R. M. Wellard, M. Woodruff, and T. Klein, "Tailoring hydrogel viscoelasticity with physical and chemical crosslinking," *Polymers (Basel).*, vol. 7, no. 12, pp. 2650–2669, 2015, doi: 10.3390/polym7121539.

[77] M. Zhou, B. H. Lee, and L. P. Tan, "A dual crosslinking strategy to tailor rheological properties of gelatin methacryloyl," *Int. J. Bioprinting*, vol. 3, no. 2, pp. 130–137, 2017, doi: 10.18063/IJB.2017.02.003.

[78] J. Ahmed, *Rheological Properties of Gelatin and Advances in Measurement*. Elsevier Ltd, 2017.

[79] M. R. Berthold *et al.*, "KNIME: The Konstanz information miner," *Stud. Classif. Data Anal. Knowl. Organ.*, pp. 319–326, 2008, doi: 10.1007/978-3-540-78246-9_38.

[80] C. Pereira, F. Araújo, C. C. Barrias, P. L. Granja, and B. Sarmento, "Dissecting stromal-epithelial interactions in a 3D invitro cellularized intestinal model for permeability

studies," *Biomaterials*, vol. 56, pp. 36–45, 2015, doi: 10.1016/j.biomaterials.2015.03.054.

[81]   R. G. Wells, "The role of matrix stiffness in regulating cell behavior," *Hepatology*, vol. 47, no. 4, pp. 1394–1400, 2008, doi: 10.1002/hep.22193.

[82]   T. Z. et Al., "d M pt," *J. Phys. D Appl. Phys.*, no. Ii, p. https://doi.org/10.1088/1361-6463/aad7de, 2018.

[83]   Y. Lei, S. Gojgini, J. Lam, and T. Segura, "The spreading, migration and proliferation of mouse mesenchymal stem cells cultured inside hyaluronic acid hydrogels," *Biomaterials*, vol. 32, no. 1, pp. 39–47, 2011, doi: 10.1016/j.biomaterials.2010.08.103.

[84]   M. Miron-Mendoza, E. Graham, S. Manohar, and W. M. Petroll, *Fibroblast-fibronectin patterning and network formation in 3D fibrin matrices*, vol. 64. Elsevier B.V., 2017.

[85]   G. Theocharidis *et al.*, "Type VI collagen regulates dermal matrix assembly and fibroblast motility," *J. Invest. Dermatol.*, vol. 136, no. 1, pp. 74–83, 2016, doi: 10.1038/JID.2015.352.

[86]   K. A. Deo, K. A. Singh, C. W. Peak, D. L. Alge, and A. K. Gaharwar, "Bioprinting 101: Design, Fabrication, and Evaluation of Cell-Laden 3D Bioprinted Scaffolds," *Tissue Eng. - Part A*, vol. 26, no. 5–6, pp. 318–338, 2020, doi: 10.1089/ten.tea.2019.0298.

[87]   E. Mancha Sánchez *et al.*, "Hydrogels for Bioprinting: A Systematic Review of Hydrogels Synthesis, Bioprinting Parameters, and Bioprinted Structures Behavior," *Front. Bioeng. Biotechnol.*, vol. 8, no. August, 2020, doi: 10.3389/fbioe.2020.00776.

[88]   K. Hölzl, S. Lin, L. Tytgat, S. Van Vlierberghe, L. Gu, and A. Ovsianikov, "Bioink properties before, during and after 3D bioprinting," *Biofabrication*, vol. 8, no. 3, 2016, doi: 10.1088/1758-5090/8/3/032002.

[89]   Y. He, F. Yang, H. Zhao, Q. Gao, B. Xia, and J. Fu, "Research on the printability of hydrogels in 3D bioprinting," *Sci. Rep.*, vol. 6, pp. 1–13, 2016, doi: 10.1038/srep29977.

[90]   C. Jimenez-Mallebrera *et al.*, "A comparative analysis of collagen VI production in muscle, skin and fibroblasts from 14 Ullrich congenital muscular dystrophy patients with dominant and recessive COL6A mutations," *Neuromuscul. Disord.*, vol. 16, no. 9–10, pp. 571–582, 2006, doi: 10.1016/j.nmd.2006.07.015.

[91] A. Bazaga, M. Roldán, C. Badosa, C. Jiménez-Mallebrera, and J. M. Porta, "A Convolutional Neural Network for the automatic diagnosis of collagen VI-related muscular dystrophies," *Appl. Soft Comput. J.*, vol. 85, p. 105772, 2019, doi: 10.1016/j.asoc.2019.105772.

[92] M. Petreaca and M. Martins-Green, "Cell–Extracellular Matrix Interactions in Repair and Regeneration," *Princ. Regen. Med.*, pp. 15–35, 2019, doi: 10.1016/b978-0-12-809880-6.00002-3.

[93] S. Hanasoge and M. Ljungman, "H2AX phosphorylation after UV irradiation is triggered by DNA repair intermediates and is mediated by the ATR kinase," *Carcinogenesis*, vol. 28, no. 11, pp. 2298–2304, 2007, doi: 10.1093/carcin/bgm157.

6 Acknowledgements

Throughout the project development and the writing of the thesis, I have received excellent assistance and support. First of all, I would like to thank my supervisors, Professor Oscar Castaño Linares, for proposing me the project and for his feedback, guidance and suggestions during these months, and Professor Valeria Chiono, to give me the opportunity to do my final master thesis at the University of Barcelona.

I would also express my gratitude to Enrico for your support, your patient guidance and all the teachings and advice given to me. Moreover, I want to thank all the Nanobioengineering group at IBEC for welcoming and integrating me since the first day. Especially, I would like to thank Inês and Sujey for all the advice and suggestions given to me and for always being ready to give a smile. Also, I would like to acknowledge all my lab mates; thank you, Miriam, Jessica, Clara, Albert, Fernando, Francesc, Ana, Andrea and Marta.

In addition, I would like to thank my family and friends.

Thanks to my mum for always being there for me, always being ready to listen to my problems, try to help me, and believe so much in me. Thanks to my dad for always encouraging and supporting me and opening my mind to the engineering world since I was a child. Thanks to my uncles, Patty, Max and Sara, to my cousins Becky, Giando and Marta. I love you all so much.

Thanks to my love, Marco, for making the university years the most incredible of my life. Thanks to Laura, Giancarlo, Giuli, Mari and Gabri, for welcoming me and making me feel part of your family.

Thanks to my best friends, Alice, Sara and Giulia, to be the essential support, to all the adventures and all the good times we had together. These years wouldn't have been the same without you.

Thanks to Canna for all the help give me during these years and for being the best university mate I could ask.

Thanks to my old friends, Kevin, Gibi, Cere, Deb, Ico, Fab, Kotia, Marti and Ciesku.

Thanks to my new friends, Elisa, Claire, Anatole, Gautier, Salman, Leonardo and Ari, for making this Erasmus so special.

Thanks to my grandparents, I know that you are with me from the stars. I give you everything, including this thesis.